Incoherent pion photoproduction on the deuteron in the first resonance region

M. I. Levchuk
B. I. Stepanov Institute of Physics, 220072 Minsk, Belarus

A. Yu. Loginov, A. A. Sidorov, and V. N. Stibunov
Nuclear Physics Institute, RU-634050 Tomsk, Russia

M. Schumacher
Zweites Physikalisches Institut, Universität Göttingen D-37077 Göttingen, Germany
(Received 15 January 2006; published 31 July 2006)

Incoherent pion photoproduction on the deuteron is studied in the first resonance region. The unpolarized cross section, the beam asymmetry, and the vector and tensor target asymmetries are calculated in the framework of a diagrammatic approach. Pole diagrams and one-loop diagrams with *NN* scattering in the final state are taken into account. An elementary operator for pion photoproduction on the nucleon is taken in various on-shell forms and calculated using the SAID and MAID multipole analyses. Model dependence of the obtained results is discussed in some detail. A comparison with predictions of other works is given. Although a reasonable description of many available experimental data on the unpolarized total and differential cross sections and photon asymmetry has been achieved, in some cases a significant disagreement between the theory and experiment has been found. Invoking known information on the reactions $\gamma d \to \pi^0 d$ and $\gamma d \to np$ we predict the total photoabsorption cross section for deuterium. We find that our values strongly overestimate experimental data in the vicinity of the Δ peak.

DOI: 10.1103/PhysRevC.74.014004 PACS number(s): 13.60.Le, 21.45.+v, 25.20.Lj

I. INTRODUCTION

Comprehensive measurements of total and differential cross sections of inclusive, coherent, and incoherent π^0 photoproduction from the deuteron in the energy region from 140 to 792 MeV were carried out at MAMI [1,2]. It was found that the coherent data are in good agreement with theoretical predictions. However, in the case of the incoherent cross sections the situation was found to be much less satisfactory. The theoretical predictions from Refs. [3,4] in the Δ region exceeded the experimental data significantly.

The above-mentioned disagreement may be indicative of shortcomings in the approaches of Refs. [3,4]. The model developed in Ref. [4] seems to be oversimplified because it takes into account the pole diagrams only. It is known that nucleon-nucleon final-state interaction (FSI) is extremely important in incoherent pion photoproduction especially for small pion angles (see, e.g., Refs. [3,5,6]). Although FSI was incorporated in the model of Ref. [3], it nevertheless failed to reproduce the data. A possible reason for this might be that Laget used in his calculations of the $\gamma d \to \pi^0 np$ process the well-known Blomqvist-Laget (BL) parametrization [7] of the pion photoproduction amplitude on the nucleon. This parametrization gives a good fit to the amplitude of charged pion photoproduction. But it does not provide a satisfactory description of π^0 production from the proton. Because data on π^0 production from the neutron are absent there is no possibility to check the reliability of the BL model in the description of this channel. An attempt to remedy this defect made in Ref. [8] led to a π^0 photoproduction operator that is not very suitable for the use in nuclear calculations.

This unsatisfactory situation has stimulated a number of new theoretical investigations of the reaction $d(\gamma, \pi)NN$ [9–18]. In Ref. [9], a computation of the differential and total cross sections for this process in the first resonance region was presented. The main difference between the approaches from Refs. [9] and [3] was that a more realistic version of an elementary pion photoproduction operator was used in the former. It was taken in the standard CGLN form [19] with four partial amplitudes F_i calculated with the use of the SAID [20] and MAID [21] multipole analyses. The model provided a satisfactory description of the data from Refs. [1,2]. Unfortunately, in Ref. [9] there was an error in coding the amplitude for the charged channels so that the reasonable description of data on the π^- channel should be considered as accidental.

In a series of articles by Darwish *et al.* [10–16], the study of incoherent pion photoproduction in the Δ-resonance region was continued. The authors used the elementary operator proposed in Ref. [4], which is quite similar to the BL operator except for slight differences in parameter values. Reasonable description of the available data on the total and differential cross sections was achieved in Ref. [11]. For the first time, an attempt to analyze polarization observables in the reaction $d(\gamma, \pi)NN$ was made in Refs. [12–16]. The beam asymmetry Σ for linearly polarized photons, target asymmetries T_{IM}, and beam-target asymmetries were discussed in those articles. However, many conclusions drawn at the analysis of the polarizations were wrong as it was explained in full detail in Ref. [17].

One more analysis of this process was presented in Ref. [17] where formal expressions for observables in incoherent pion photoproduction were given, as well as in a subsequent article [18]. Using the MAID model for an elementary production operator, the authors studied the inclusive reaction from threshold up to 1 GeV. They obtained quite satisfactory

agreement with the data similar to that achieved in Refs. [12–16] although considerable deviation from the predictions of the latter articles was found for many polarization asymmetries. A part of the deviation is a consequence of the use of wrong formal expressions in those articles. But in the cases when the right expressions were used, the origin of the deviation remained to be unclear.

It should be noted that in neither of the works [11–16,18], the question on model dependencies of the calculations was studied. Only the sensitivity of the predictions to the choice of the model for NN interaction was investigated and was found to be very small. An analogous result was also reported in Ref. [9]. But the dependencies mentioned do exist. They mainly stem from the elementary production operator. First, two now-available multipole analyses, SAID and MAID, are not equivalent and give different results for observables. The size of the deviation depends on the kinematic region and on the observable under consideration. For example, the total cross sections produced by the SAID SM04K solution at the total energy of 1232 MeV are 267, 270, 212, and 240 μb for the $\pi^0 p, \pi^0 n, \pi^+ n$, and $\pi^- p$ channels, respectively. The corresponding numbers given by the MAID03 solution are 279, 281, 215, and 244 μb. It is clear that this sensitivity to the choice of the analysis will be seen in the reaction $d(\gamma,\pi)NN$ too. Even different solutions for the same analysis (e.g., MAID00 or MAID03) give different results that leads to additional model dependence in this reaction. Second, both the SAID and MAID models are the parametrizations of an on-shell production operator. The latter depends on four invariant amplitudes [19]. Different options are possible for these amplitudes that are equivalent in the on-shell case. However, this equivalence is broken in deuteron (or more generally, in nuclear) calculations when one nucleon or both of them are off their mass shells. Though it is difficult to give precise numerical account for the off-shell effects, we should at least estimate possible uncertainties of the results introduced by them.

We, therefore, motivate the present work by the following reasons. First, we compare our results with those from Refs. [11–16] and Ref. [18] in the framework of an analogous approach, i.e., in the impulse approximation with FSI effects, because any new calculation can serve as an independent check of which of the above models is valid. Second, we want to estimate possible uncertainties in theoretical predictions for observables. These uncertainties should be kept in mind when extracting information on the amplitude of pion photoproduction on the neutron from deuteron data.

The article is organized as follows. In Sec. II, the kinematic relations used for the calculations and definitions for observables are briefly reviewed. A description of the theoretical model and its ingredients is given in Sec. III. Section IV contains the results on the differential and total cross sections as well as beam and target asymmetries with a special emphasis on possible uncertainties of the results. In the same section we also compare our predictions with data available in the considered kinematic region and with results of other approaches given in Refs. [11–16,18]. Different parametrizations for the elementary photoproduction operator are presented in Appendix A.

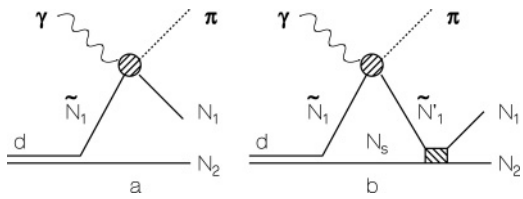

FIG. 1. Diagrams considered in this work. Two other diagrams with the permutation $1 \leftrightarrow 2$ are assumed.

II. KINEMATICS AND DEFINITIONS OF OBSERVABLES

Let us denote by $k = (k^0, \vec{k})$, $p_d = (\varepsilon_d, \vec{p}_d)$, $q = (\varepsilon_\pi, \vec{q})$, $p_1 = (\varepsilon_1, \vec{p}_1)$, and $p_2 = (\varepsilon_2, \vec{p}_2)$ the four-momenta of the initial photon and deuteron and the final pion and nucleons, respectively. A symbol E_γ is reserved for the lab photon energy ($k^0_{\rm lab} = E_\gamma$) and a symbol ω will be used for the photon energy in the γd center-of-mass (c.m.) frame ($k^0_{\rm c.m.} = \omega = E_\gamma M / W_{\gamma d}$) with $W_{\gamma d} = \sqrt{M^2 + 2ME_\gamma}$ and M being the deuteron mass.

We take as independent kinematic variables the photon energy and pion momentum $\vec{q}$ in the used frame of reference (generally, the lab or c.m. frame) and the angles $\Theta_{\vec{P}}$ and $\phi_{\vec{P}}$ of one of the nucleons in the c.m. frame of the final nucleon-nucleon pair. Using the equality

$$W_{NN} = 2\varepsilon_P = 2\sqrt{\vec{P}^2 + m^2} = \sqrt{(k + p_d - q)^2}, \qquad (1)$$

where m is the nucleon mass, one can find the momentum $\vec{P}$. After boosting the momenta $\vec{P}$ and $-\vec{P}$ with the velocity $(\vec{k} + \vec{p}_d - \vec{q})/(k^0 + \varepsilon_d - \varepsilon_\pi)$ the momenta of the outgoing nucleons are obtained and, therefore, the kinematics is totally determined.

The differential cross section is given by

$$\frac{d\sigma}{d\vec{q}\, d\Omega_{\vec{P}}} = \frac{1}{(2\pi)^5} \frac{m^2 \varepsilon_d |\vec{P}|}{8k \cdot p_d\, \varepsilon_\pi \varepsilon_P} \frac{1}{6} \sum_{m_2 m_1 \lambda m_d} |\langle m_2 m_1 | T | \lambda m_d \rangle|^2, \qquad (2)$$

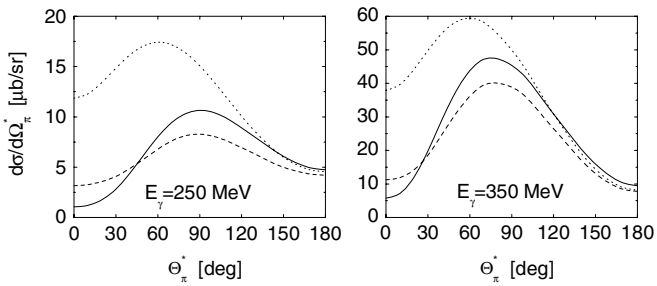

FIG. 2. Differential cross section for the reaction $d(\gamma,\pi^0)np$ in the c.m. frame at 250 and 350 MeV. The dotted curves are the results without FSI. Only the "on-shell part" of the contribution of the diagram in Fig. 1(b) is retained in the dashed curves. Addition of the "off-shell part" gives the solid curves.

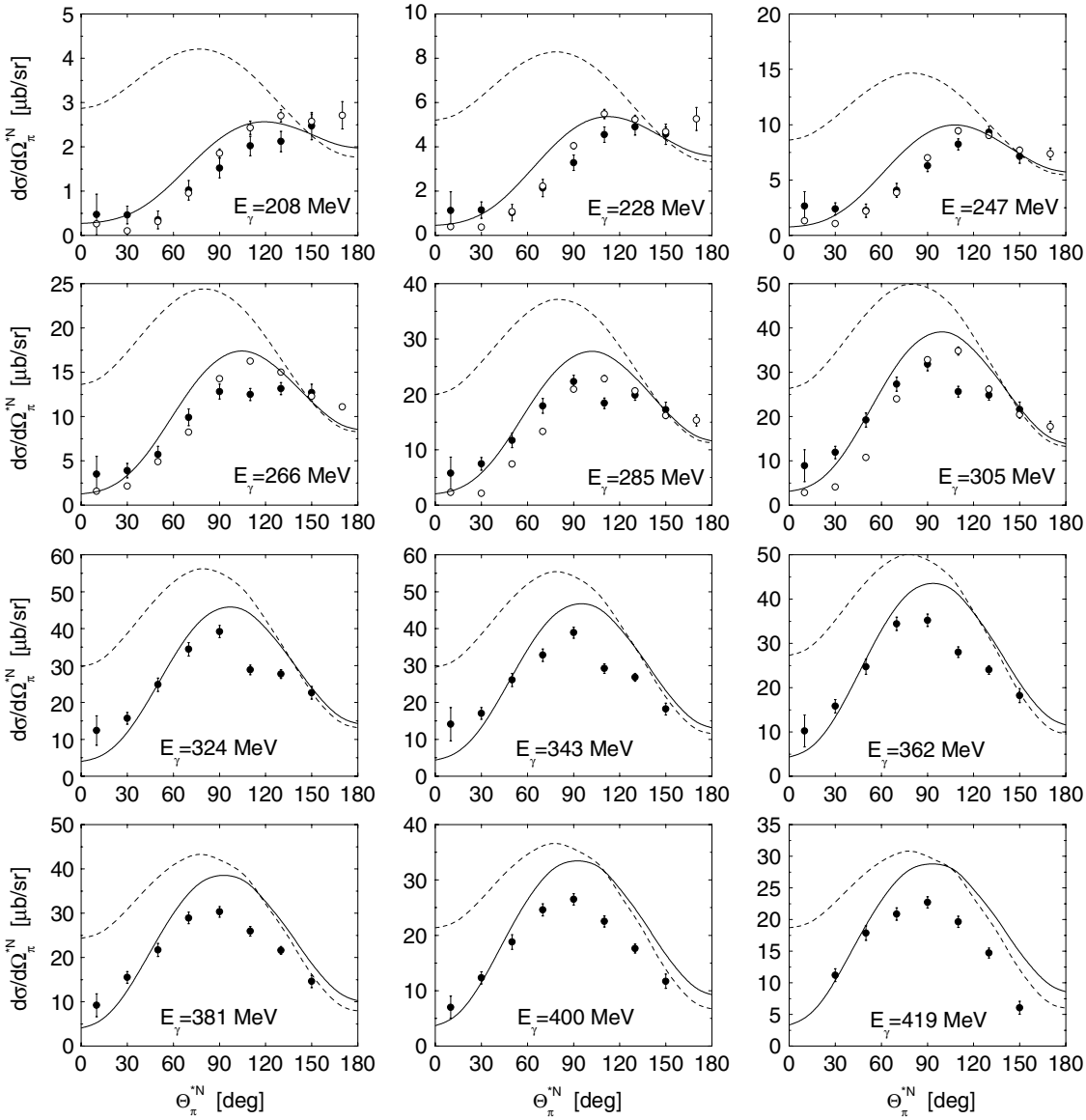

FIG. 3. Differential cross section for π^0 production in the photon-nucleon c.m. frame obtained with the FA04K solution of the SAID analysis and with the parametrization of the production operator through the invariant amplitudes A_i. The dotted (solid) curves are our predictions without (with) FSI. Data are from Ref. [1] (●) and Ref. [2] (○).

where m_2, m_1, λ, and m_d are spin states of the two nucleons, photon, and deuteron, respectively. To obtain the inclusive differential cross section $d\sigma/d\Omega_\pi$, the right-hand side (rhs) of Eq. (2) has to be integrated over the value of the pion momentum $q = |\vec{q}|$ and the solid angle $\Omega_{\vec{P}}$

$$\frac{d\sigma}{d\Omega_\pi} = \int_{q^{\min}}^{q^{\max}} q^2 dq \int d\Omega_{\vec{P}} \frac{d\sigma}{d\vec{q}\, d\Omega_{\vec{P}}} = \frac{1}{6} S, \tag{3}$$

where S is defined as

$$S = \int_{q\min}^{q\max} f q^2 dq \int d\Omega_{\vec{\mathbf{P}}} \sum_{m_2 m_1 \lambda m_d} |\langle m_2 m_1 | T | \lambda m_d \rangle|^2, \tag{4}$$

with

$$f = \frac{1}{(2\pi)^5} \frac{m^2 \varepsilon_d |\vec{P}|}{8k \cdot p_d\, \varepsilon_\pi \varepsilon_P}. \tag{5}$$

An extra factor of 1/2 must be included in the rhs of Eq. (3) in case of charged pion photoproduction. The maximum value $q^{\max}$ can be found from Eq. (1) at $W_{NN} = 2m$. In the c.m. frame it is given by

$$\begin{aligned} q^{\max} &= \frac{1}{2W_{\gamma d}} \sqrt{\left[W_{\gamma d}^2 - (2m+\mu)^2\right]\left[W_{\gamma d}^2 - (2m-\mu)^2\right]}, \\ q^{\min} &= 0, \end{aligned} \tag{6}$$

where μ is the pion mass. In the lab frame one has

$$\begin{aligned} q^{\max} &= q^{\max}(\Theta_\pi) = \frac{1}{b}[a E_\gamma z + (E_\gamma + M)\sqrt{a^2 - b\mu^2}], \\ q^{\min} &= q^{\min}(\Theta_\pi) \\ &= \min\left(0, \frac{1}{b}[a E_\gamma z - (E_\gamma + M)\sqrt{a^2 - b\mu^2}]\right), \end{aligned} \tag{7}$$

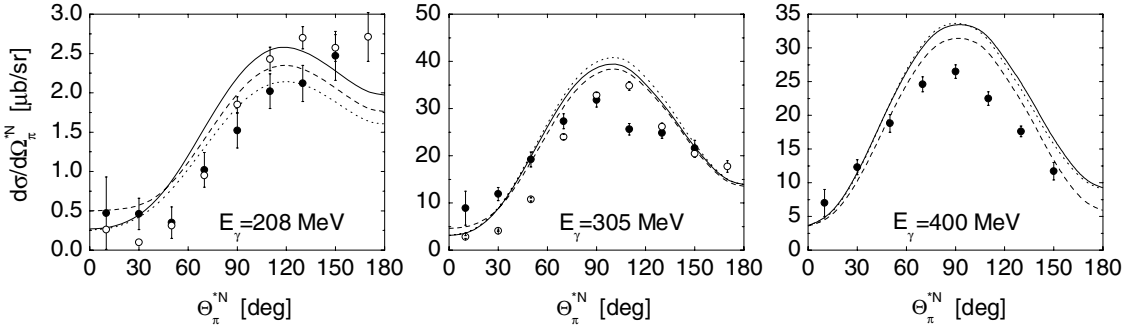

FIG. 4. Differential cross section for the π^0 channel in the photon-nucleon c.m. frame with different parametrizations of the production operator: dashed and solid curves are obtained with the amplitudes A_i' and A_i, respectively, for the SAID FA04K solution. Dotted curves are obtained with the amplitudes A_i and the MAID03 solution. Data as described in the legend to Fig. 3.

where $a = (W_{\gamma d}^2 - 4m^2 + \mu^2)/2$ and $b = (E_\gamma + M)^2 - E_\gamma^2 z^2$ with $z = \cos\Theta_\pi$. Note that the inequality $q^{\min} \neq 0$ can take place only for $\Theta_\pi \leqslant 90^\circ$, and at threshold energies

$$E_\gamma < E_\gamma^{\max} = \frac{4m^2 - (M-\mu)^2}{2(M-\mu)}. \tag{8}$$

The energy $E_\gamma^{\max}$ is equal to 142.6 [if one takes $m = (m_p + m_n)/2 = 938.9$ MeV], 149.0, and 146.2 MeV for π^0, π^+, and π^- channels, respectively. Therefore, in the considered energy region, $q^{\min}$ is equal to zero also in the lab frame.

Apart from the differential cross section, single polarization observables will be considered in the article, namely the photon beam asymmetry Σ and target asymmetries $T_{\rm IM}$. Below, we give their definitions through the reaction amplitude (see also Ref. [17]). The photon asymmetry is

$$\sum = \frac{(d\sigma/d\Omega_\pi)^{\parallel} - (d\sigma/d\Omega_\pi)^{\perp}}{(d\sigma/d\Omega_\pi)^{\parallel} + (d\sigma/d\Omega_\pi)^{\perp}} = -\frac{1}{S}\, 2 \int_{q\,\min}^{q\,\max} f q^2 dq \times \int d\Omega_{\vec{p}} \mathrm{Re} \sum_{m_2 m_1 m_d} \langle m_2 m_1 | T | + 1 m_d \rangle \times \langle m_2 m_1 | T | - 1 m_d \rangle^*, \tag{9}$$

where $(d\sigma/d\Omega_\pi)^{\parallel(\perp)}$ is the inclusive cross section for the photons polarized parallel (perpendicular) to the xz plane. Note that the minus sign in the rhs of Eq. (9) is absent in the corresponding formulas from Refs. [12–16]. The deuteron vector asymmetry T_{11} and tensor asymmetries T_{2M} are as

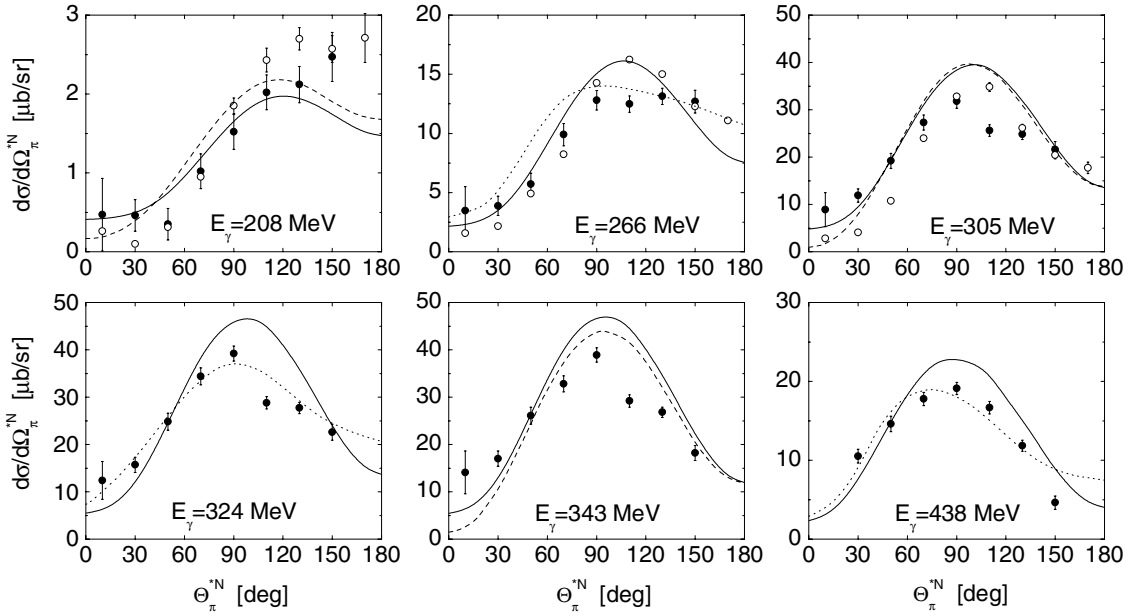

FIG. 5. Differential cross section for the reaction $d(\gamma, \pi^0)np$ in the photon-nucleon c.m. frame obtained in three models: the present calculation with the amplitudes A_i' and the MAID03 solution (solid), Ref. [11] (dotted), and Ref. [18] (dashed). Data as described in the legend to Fig. 3.

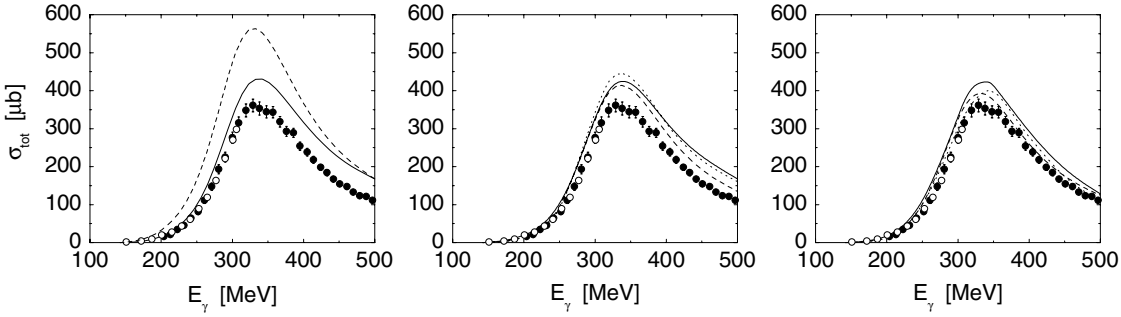

FIG. 6. Total cross section for the reaction $d(\gamma,\pi^0)np$. (Left panel) Results with the FA04K solution of the SAID analysis and with the parametrization of a pion production operator through the invariant amplitudes A_i. The dotted (solid) curves are the predictions without (with) FSI. (Middle panel) Dashed and solid curves are obtained with the amplitudes A_i' and A_i, respectively, for the SAID FA04K solution. The dotted curve is obtained with the amplitudes A_i and the MAID03 solution. (Right panel) The present calculation with the amplitudes A_i' and the MAID03 solution (solid), Ref. [11] (dotted), and Ref. [18] (dashed). Data as described in the legend to Fig. 3.

follows [1]

$$
\begin{aligned}
T_{11} &= \frac{1}{S}\sqrt{6}\int_{q\,\min}^{q\,\max} f q^2 dq \int d\Omega_{\vec{P}} \\
&\quad \times \mathrm{Im}\sum_{m_2 m_1 \lambda} (\langle m_2 m_1|T|\lambda+1\rangle - \langle m_2 m_1|T|\lambda-1\rangle) \\
&\quad \times \langle m_2 m_1|T|\lambda 0\rangle^*, \\
T_{20} &= \frac{1}{S}\frac{1}{\sqrt{2}}\int_{q\,\min}^{q\,\max} f q^2 dq \int d\Omega_{\vec{P}} \\
&\quad \times \sum_{m_2 m_1 \lambda} (|\langle m_2 m_1|T|\lambda-1\rangle|^2 + |\langle m_2 m_1|T|\lambda+1\rangle|^2 \\
&\quad - 2|\langle m_2 m_1|T|\lambda 0\rangle|^2), \\
T_{21} &= \frac{1}{S}\sqrt{6}\int_{q\,\min}^{q\,\max} f q^2 dq \int d\Omega_{\vec{P}} \\
&\quad \times \mathrm{Re}\sum_{m_2 m_1 \lambda} (\langle m_2 m_1|T|\lambda-1\rangle - \langle m_2 m_1|T|\lambda+1\rangle) \\
&\quad \times \langle m_2 m_1|T|\lambda 0\rangle^*, \\
T_{22} &= \frac{1}{S}2\sqrt{3}\int_{q\,\min}^{q\,\max} f q^2 dq \int d\Omega_{\vec{P}} \\
&\quad \times \mathrm{Re}\sum_{m_2 m_1 \lambda} \langle m_2 m_1|T|\lambda-1\rangle\langle m_2 m_1|T|\lambda+1\rangle^*. \qquad (10)
\end{aligned}
$$

III. THE THEORETICAL MODEL FOR INCLUSIVE PION PHOTOPRODUCTION ON THE DEUTERON

The diagrammatic approach is exploited to calculate the amplitude $\langle m_2 m_1|T|\lambda m_d\rangle$ in Eq. (2). In comparison with Refs. [5,6], we reduce the set of diagrams under consideration. For example, in Ref. [6] where the threshold region was considered, a two-loop diagram that includes simultaneously np and πN interactions had to be taken into account. Such a diagram is of importance at threshold energies because it involves a block with charged pion photoproduction from the nucleon. With increasing photon energy this diagram becomes less important as it was shown in Ref. [6]. Above 200 MeV it can safely be disregarded. It is known (see Refs. [3,22]) that there are kinematic regions where a one-loop diagram with πN rescattering noticeable contributes to the amplitude. But this rather concerns the exclusive process $\gamma d \to \pi NN$. We have checked that πN rescattering changes the final results in the first resonance region by only a few percentages.

As a result, we retain in our calculations the two diagrams shown in Fig. 1. The pole diagram 1(a) must be taken into account because at the integrations in Eq. (3), one goes through the kinematic regions where the relative momentum $(\vec{\tilde{p}}_1 - \vec{p}_2)/2$ is small and, therefore, the deuteron wave function (DWF) has its maximum. These are the so-called quasifree regions. The exclusive cross section has sharp peaks in these regions. Here the inclusive cross section from the pole diagrams is mainly saturated. It is worth mentioning that in the peak regions the active nucleon $\tilde{N}_1$ is almost on its mass shell. In the center of the peaks the difference between on-shell and off-shell energies of this nucleon is equal to the deuteron binding energy $\Delta = 2.2$ MeV. Therefore, the use of the on-shell parametrization for a pion photoproduction operator is justified when considering diagram in Fig. 1(a). Nevertheless, as shown below, the off-shell dependence of calculated observables does exist even when one considers contributions from the pole diagram in Fig. 1(a).

Another important mechanism is displayed in Fig. 1(b). When at the mentioned integration the relative momentum of the outgoing nucleons, $\vec{p}_{\rm out} = (\vec{p}_2 - \vec{p}_1)/2$, decreases, there are peaks in the exclusive cross sections because of strong final state NN interaction in the s waves (see, e.g., Refs. [3,5,22]). The peaks reveal themselves in a big contribution of diagram 1(b) to the inclusive cross section. The effect of this diagram is expected to be most pronounced at small pion angles because in this case the low-momentum regime simultaneously for both DWF and NN scattering amplitude is kinematically permitted. The possibility of using the on-shell parametrization for the pion photoproduction amplitude at evaluation of the diagram 1(b) is less evident and it is discussed below.

[1] The opposite sign for T_{11} is used in Refs. [12,16].

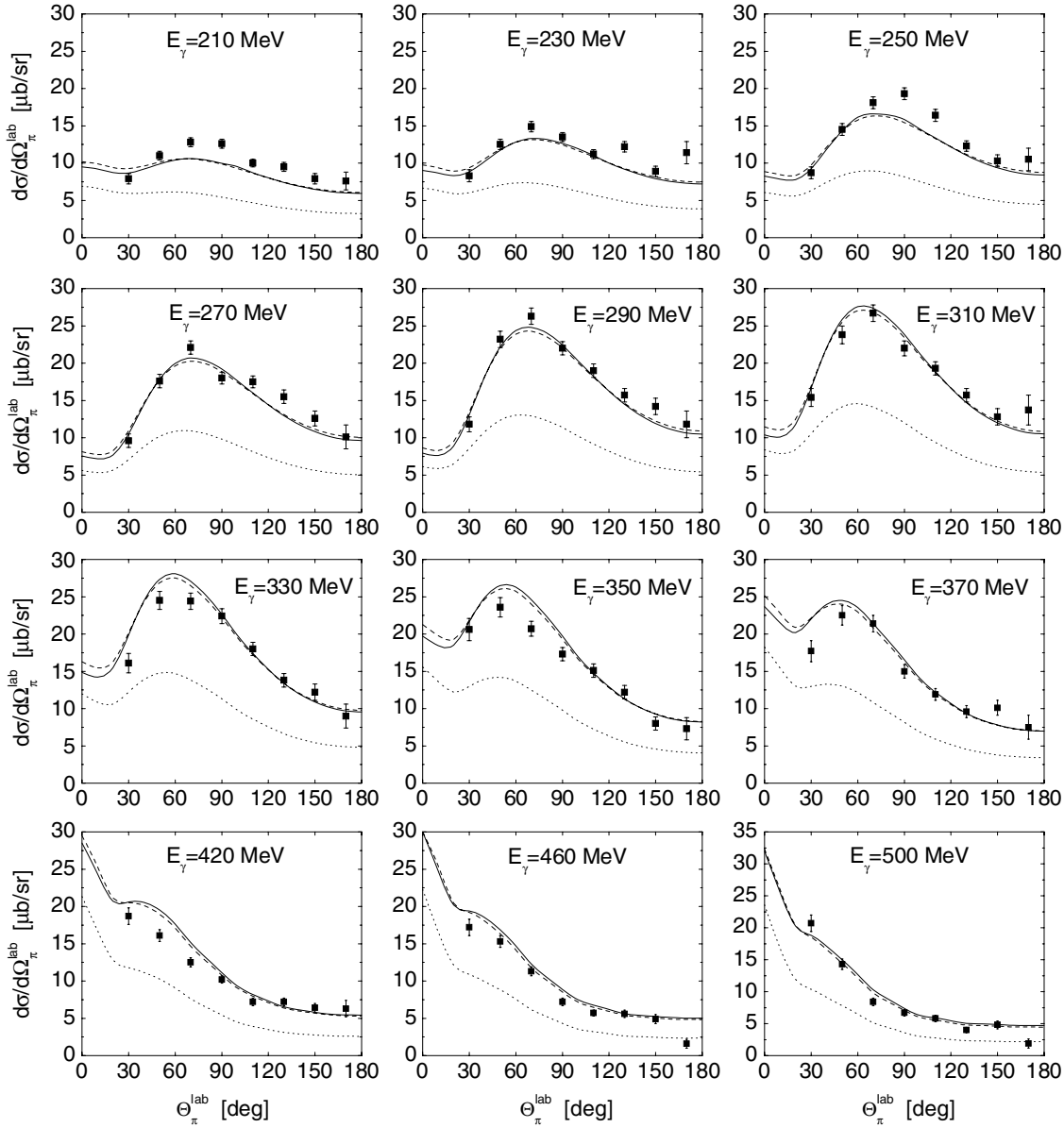

FIG. 7. Differential cross section for the reaction $d(\gamma,\pi^-)pp$ in the lab frame obtained with the amplitudes A_i and the SAID FA04K solution. The dotted curves are contributions from one of the pole diagrams in Fig. 1. Successive addition of the second pole diagram and FSI leads to dashed and solid curves, respectively. Data are from Ref. [31].

Let us now write out the matrix elements corresponding to the diagrams in Fig. 1 (see also Refs. [3,6,11,18,22]). One has for the pole diagram in Fig. 1(a)

$$\langle m_2 m_1|T^a(p_2,\,p_1,\,q;k)|\lambda m_d\rangle = \sum_{\tilde{m}_1}\Psi^{m_d}_{m_2\tilde{m}_1}\left(\vec{p}_2-\frac{\vec{p}_d}{2}\right) \times \langle m_1|T_{\gamma\tilde{N}_1\to\pi N_1}(p_1,\,q;\,\tilde{p}_1,\,k)|\lambda\tilde{m}_1\rangle, \tag{11}$$

where $\Psi^{m_d}_{m_2\tilde{m}_1}(\vec{p}_2-\vec{p}_d/2)$ is DWF and $\langle m_1|T_{\gamma\tilde{N}_1\to\pi N_1}(p_1,\,q;\,\tilde{p}_1,\,k)|\lambda\tilde{m}_1\rangle$ is the amplitude of pion photoproduction on the nucleon. There is one more pole diagram identical to that in Fig. 1(a) but with the replacement $1\leftrightarrow 2$. In case of π^0 production the corresponding matrix element should be added to Eq. (11). For the charged channels a subtraction of two matrix elements should be done.

The deuteron wave function reads

$$\Psi^{m_d}_{m_2\tilde{m}_1}(\vec{p}) = (2\pi)^{3/2}\left[\frac{1}{\sqrt{4\pi}}C^{1m_d}_{\frac{1}{2}m_2\frac{1}{2}\tilde{m}_1}u(p) - C^{1m_S}_{\frac{1}{2}m_2\frac{1}{2}\tilde{m}_1} \times C^{1m_d}_{2m_L1m_S}Y_2^{m_L}(\hat{\vec{p}})w(p)\right], \tag{12}$$

where $m_S = m_2+\tilde{m}_1, m_L = m_d - m_S$; $Y_2^{m_L}(\hat{\vec{p}})$ are the spherical harmonics; and $C^{JM}_{J_2M_2J_1M_1}$ are the Clebsch-Gordan coefficients. The present calculation is done using the CD-Bonn potential from Ref. [23] where analytical parametrizations of the s and d amplitudes of DWF [$u(p)$ and $w(p)$,

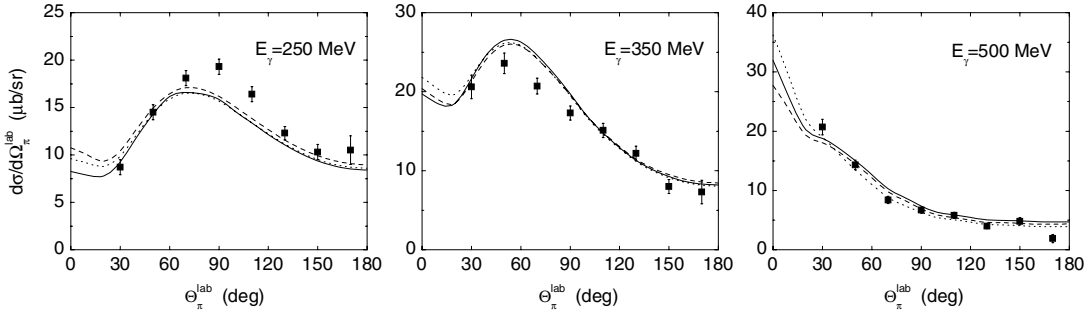

FIG. 8. Differential cross section for the reaction $d(\gamma, \pi^-)pp$ in the lab frame with different parametrizations of a production operator. Notations of the curves as in Fig. 4. Data are from Ref. [31].

respectively] is given. We note that our results are practically independent of the choice of a model for NN interaction. Calculations with three OBEPR versions of the Bonn potential [24,25] or with a separable representation [26] of the Paris potential give almost the same predictions for observables.

If it is not stated otherwise, all the results below are obtained with the production operator parametrized via the invariant amplitudes A_i. They are defined in Eqs. (A1) and (A3) and calculated with both the SAID and MAID analyses. The calculation for the SAID analysis is performed in two steps. First, the CGLN amplitudes F_i in the c.m. frame [Eq. (A7)] are found making the use of electric and magnetic multipoles predicted by the analysis. We do not give explicit expressions for F_i through the multipoles because they are very well known. Second, one finds the amplitudes A_i using the relation (A9) between A_i and F_i. The MAID group provides users directly with the amplitudes F_i for the MAID00 solution and with both F_i and A_i for the MAID03 solution.

Strictly speaking there are other possible options for the invariant amplitudes. In particular, in Ref. [18] another set of those, A'_i, as defined in Eqs. (A11) and (A12) was exploited. The production operators given by the amplitudes A_i and A'_i are equivalent in the case of on-shell nucleons as is explained in some detail in Appendix A. This equivalence is destroyed when the nucleons are off their mass shells. Because in deuteron calculations one deals with off-shell nucleons, we expect our results to be dependent on the parametrization of the elementary operator.

The matrix element corresponding to diagram 1(b) is

$$\langle m_2 m_1 | T^b(p_2, p_1, q; k) | \lambda m_d \rangle = -m \int \frac{d^3 \vec{p}_s}{(2\pi)^3} \sum_{m_s \tilde{m}'_1} \frac{\langle \vec{p}_{\rm out}, m_2 m_1 | T_{NN} | \vec{p}_{\rm in}, m_s \tilde{m}'_1 \rangle \langle m_s \tilde{m}'_1 | T^a(p_s, \tilde{p}'_1, q; k) | \lambda m_d \rangle}{p_{\rm in}^2 - p_{\rm out}^2 - i0}. \tag{13}$$

The amplitude $\langle m_s \tilde{m}'_1 | T^a(p_s, \tilde{p}'_1, q; k) | \lambda m_d \rangle$ in Eq. (13) is the same as that in Eq. (11) but with the replacements $2 \to$ s and $p_1 \to \tilde{p}'_1$. The second pole diagram mentioned above with $1 \leftrightarrow 2$ must also be included in the integrand of Eq. (13). The choice of the energy of the off-shell nucleon $\tilde{N}_1$ is discussed at the end of this section.

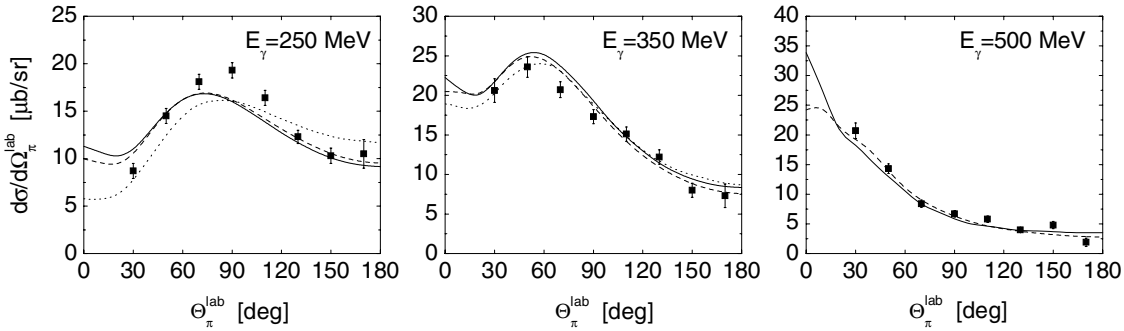

FIG. 9. Differential cross section for the reaction $d(\gamma, \pi^-)pp$ in the lab frame obtained in three models: the present calculation with the amplitudes A'_i and the MAID03 solution (solid), Ref. [11] (dotted), and Ref. [18] (dashed). Data are from Ref. [31].

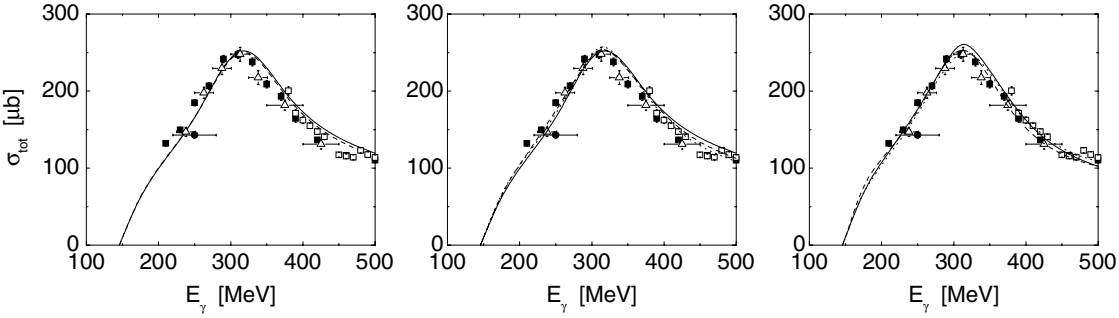

FIG. 10. Total cross section for the reaction $d(\gamma, \pi^-)pp$. Notations of the curves as in Fig. 6. Data are from Refs. [31] (■), [32] (△), [33] (□), and [34] (●).

The half-off-shell NN-scattering amplitude $\langle \vec{p}_{\rm out}, m_2 m_1 | T_{NN} | \vec{p}_{\rm in}, m_s \tilde{m}'_1 \rangle$ depends on the relative off-shell momentum of the $N_1 N_2$ pair before scattering, $\vec{p}_{\rm in} = \vec{p}_s - (\vec{p}_1 + \vec{p}_2)/2$, and the relative on-shell momentum after scattering, $\vec{p}_{\rm out} = (\vec{p}_2 - \vec{p}_1)/2$, as

$$\begin{aligned}\langle \vec{p}_{\rm out}, m_2 m_1 | T_{NN} | \vec{p}_{\rm in}, m_s \tilde{m}'_1 \rangle &= (2\pi)^3 \sqrt{\frac{\varepsilon_{\rm out}}{m}} \sqrt{\frac{\varepsilon_{\rm in}}{m}} \sum_{JSLL'm_J} C^{Sm_S}_{\frac{1}{2}m_s \frac{1}{2}\tilde{m}'_1} C^{Sm'_S}_{\frac{1}{2}m_2 \frac{1}{2}m_1} C^{Jm_J}_{Lm_L Sm_S} \\ &\times C^{Jm_J}_{L'm_{L'}Sm'_S} i^{L-L'} Y^{m_L *}_L(\hat{\vec{p}}_{\rm in}) Y^{m_{L'}}_{L'}(\hat{\vec{p}}_{\rm out}) R^{JS}_{L'L}(p_{\rm out}, p_{\rm in}),\end{aligned} \tag{14}$$

where $m_S = m_s + \tilde{m}'_1, m'_S = m_2 + m_1, m_L = m_J - m_S$, and $m_{L'} = m_J - m'_S$. The factors $\sqrt{\varepsilon_{\rm out}/m}$ and $\sqrt{\varepsilon_{\rm in}/m}$ ($\varepsilon_{\rm out} = \sqrt{p^2_{\rm out} + m^2}$ and $\varepsilon_{\rm in} = \sqrt{p^2_{\rm in} + m^2}$) come from the so-called minimal relativity. The half-off-shell partial amplitudes $R^{JS}_{L'L}(p_{\rm out}, p_{\rm in})$ were obtained by solving the Lippmann-Schwinger equation for the CD-Bonn potential. The procedure for obtaining these amplitudes is quite direct for np and nn interactions. It should be, however, modified in the case of pp interaction. First, the Coulomb interaction has to be added to pure nuclear interaction. A method to handle Coulomb interaction in momentum space was proposed by Vincent and Phatak [27]. We do not discuss it here because it is described in full detail in that article (see also Refs. [23,28,29]). We mention only that the method was applied to the $^1S_0$ partial wave. All other waves with $J = 0$ and 1 are taken for the switched off Coulomb potential. It makes no sense to include the Coulomb modifications for the waves other than $^1S_0$ because even the contribution of this latter to the observables was found to be small. As a next step, we used a prescription from Ref. [30] consisting of the following parametrization of the half-off-shell $^1S_0$ partial amplitude for pp scattering

$$R^{^1S_0}_{\rm off}(p_{\rm out}, p_{\rm in}) = \frac{p^2_{\rm out} + \beta^2}{p^2_{\rm in} + \beta^2} \quad R^{^1S_0}_{\rm on}(p_{\rm out}, p_{\rm out}), \tag{15}$$

with $\beta = 1.2$ fm^{-1}. The on-shell amplitude $R^{^1S_0}_{\rm on}(p_{\rm out}, p_{\rm out})$ is obtained with the use of the Vincent and Phatak method with switched on Coulomb interaction.

All partial waves with the total angular momentum $J \leqslant 3$ were retained in Eq. (14). In fact, however, only one wave, $^3S_1$, in the case of π^0 photoproduction is of importance. All other waves contribute a few percentages to observables. Further details of the computations of Eq. (13) can be found in Ref. [5].

Again the question emerges whether the on-shell parametrization for the pion photoproduction amplitude is applicable at calculations of the matrix element (13). To discuss this point, we point out that at the evaluation of the integral in Eq. (13) it is assumed, in accordance with a finding from Refs. [3,22], the spectator nucleon N_s to be on its mass shell. This means that the nucleon $\tilde{N}_1$ momentum is $-\vec{p}_s$ and its energy is equal to $2m - \Delta - \sqrt{p^2_s + m^2}$ (for simplicity we consider the lab frame). The integral in Eq. (13) is saturated at momenta $p_s \sim \sqrt{m\Delta}$ when DWF has its maximum. In other words, the energy of the nucleon $\tilde{N}_1$ is effectively off its on-shell value by only few multiplicities of binding energies Δ. Furthermore, using the symbolic equality

$$\frac{1}{p^2_{\rm in} - p^2_{\rm out} - i0} = \frac{i\pi}{2p_{\rm out}} \delta(p_{\rm in} - p_{\rm out}) + P \frac{1}{p^2_{\rm in} - p^2_{\rm out}}, \tag{16}$$

one can split the matrix element [Eq. (13)] in its on-shell part and its off-shell part corresponding to the first and second terms in the rhs of Eq. (16), respectively. With only the former included we calculated the cross sections and found it to give the main contribution (see Fig. 2). Taking into account that the nucleon N_s is on its mass shell, one concludes

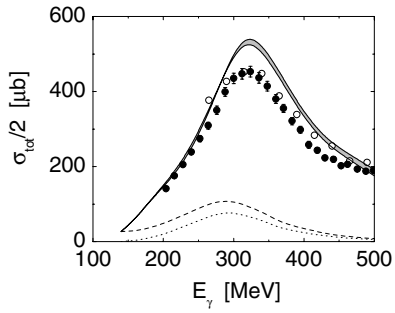

FIG. 11. Total photoabsorption cross section per nucleon for the deuteron from 150 to 500 MeV. Contribution of the reaction $\gamma d \to \pi^0 d$ is shown as dotted curve. Contribution from deuteron photodisintegration is included in dashed curve. Filled area includes contributions from all channels $\gamma d \to \pi NN$ (see text). Data are from Refs. [37] (○) and [38] (●).

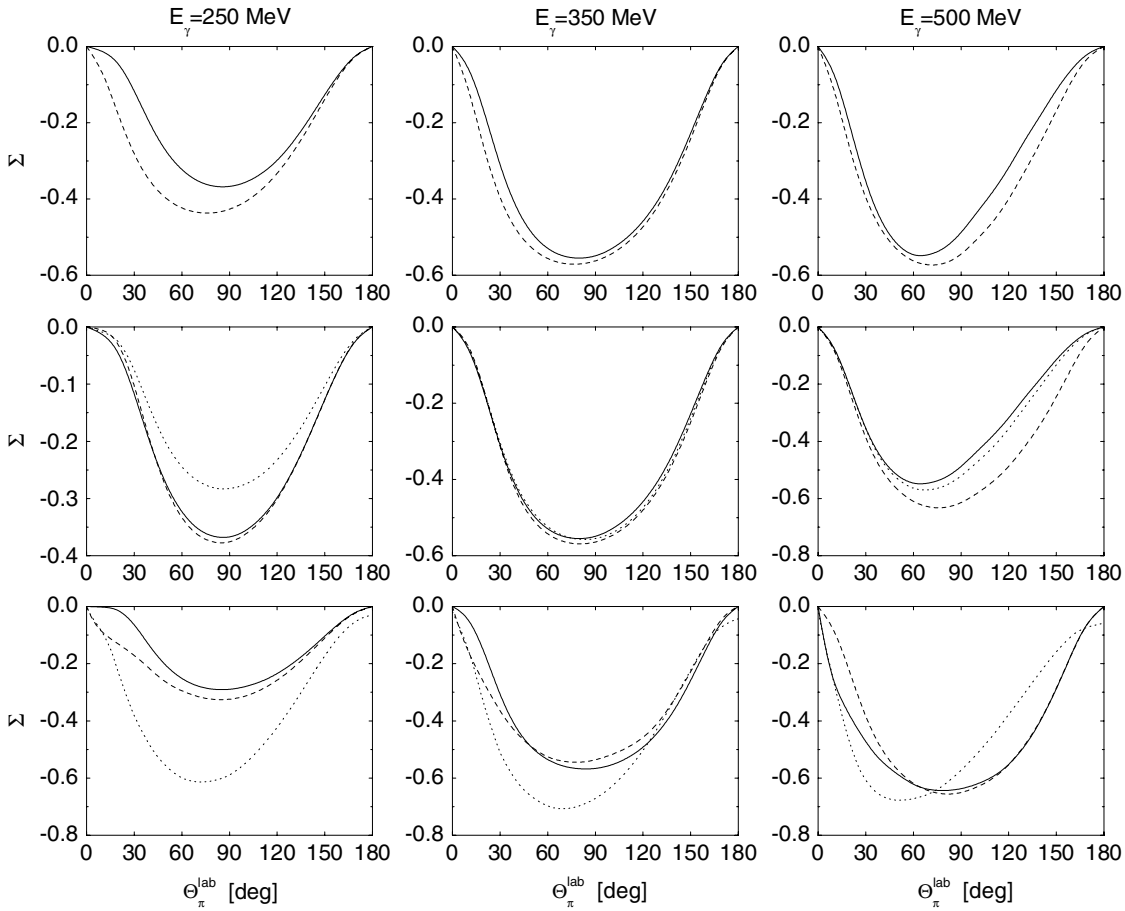

FIG. 12. Angular distribution of the asymmetry Σ for the reaction $d(\gamma, \pi^0)np$. (Upper panel) The dotted (solid) curves are our predictions without (with) FSI obtained with the SAID FA04K solution and with the amplitudes A_i. (Middle panel) Dashed and solid curves are obtained with the amplitudes A_i' and A_i, respectively, for the SAID FA04K solution. Dotted curves are obtained with the amplitudes A_i and the MAID03 solution. (Lower panel) The present calculation with the amplitudes A_i' and the MAID03 solution (solid), Refs. [12,13] (dotted), and Ref. [18] (dashed).

that this part corresponds to the case when the nucleon $\tilde{N}_1'$ is also on its mass shell. Therefore, the contribution of the amplitude Eq. (13) to the inclusive cross section comes mainly from the kinematic domains in the integrand of Eq. (13) where the nucleons $\tilde{N}_1$ and $\tilde{N}_1'$ are close to their mass shells. The same conclusion holds true also for other observables. Therefore, the on-shell parametrization for an elementary pion photoproduction operator is applicable in this integrand. Nevertheless, some dependence of the FSI amplitude [Eq. (13)] on off-shell effects is expected.

As in Refs. [5,6], all summations over polarizations of the particles in Eqs. (11) and (13) as well as the three-dimensional integration in Eq. (13) have been carried out numerically. The number of chosen nodes at this integration and that in Eq. (3)

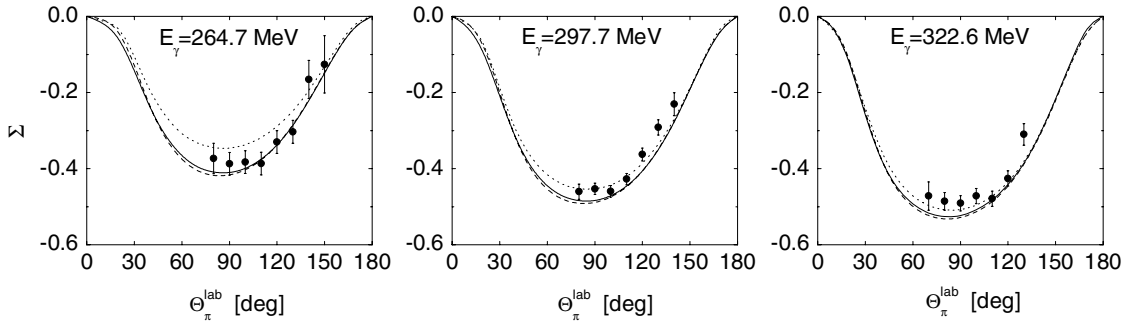

FIG. 13. Angular distribution of the asymmetry Σ for the reaction $d(\gamma, \pi^0)np$. Notation of the curves as in the middle panel of Fig. 12. Data (preliminary) are from Ref. [40].

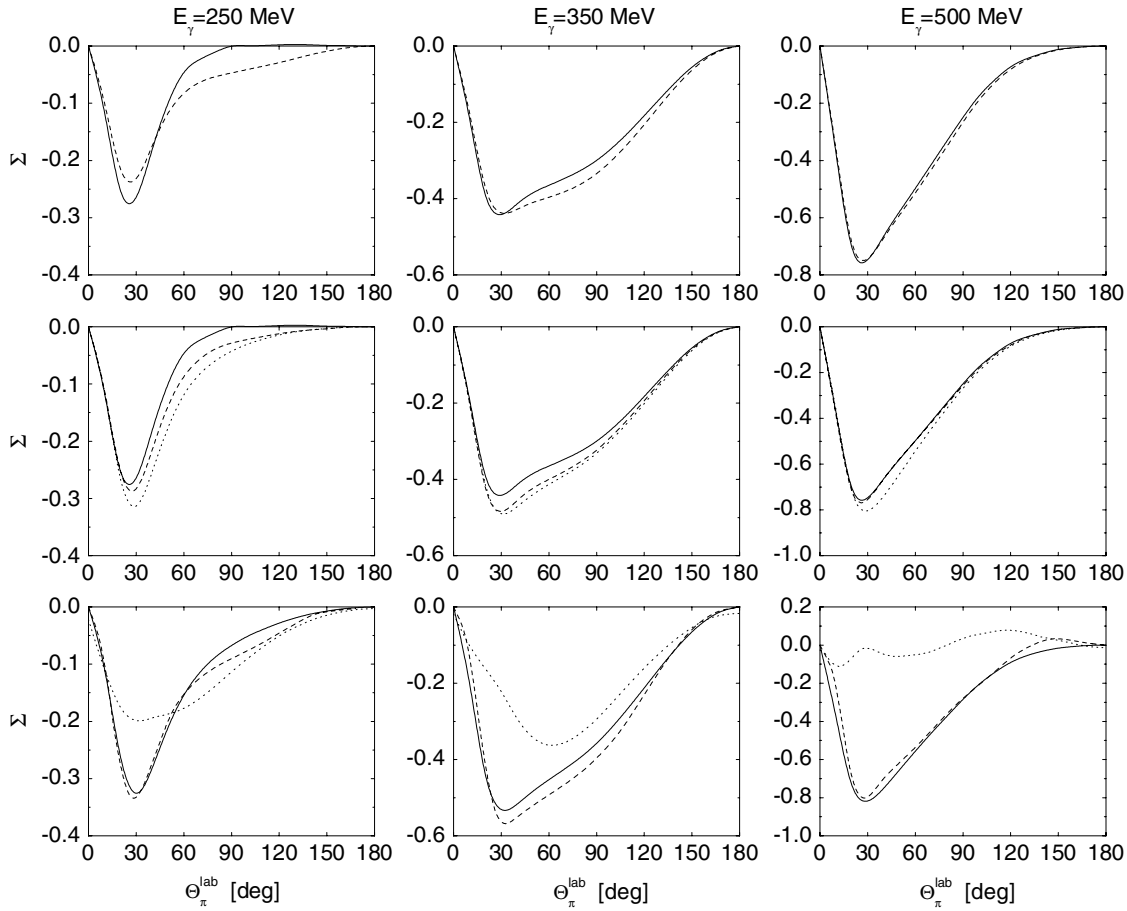

FIG. 14. Angular distribution of the asymmetry Σ for the reaction $d(\gamma, \pi^-)pp$. Notation of the curves as in Fig. 12. Results from Refs. [15,16] are shown as dotted curves of the lower panel.

were taken to be sufficient for prediction of observables with the numerical accuracy better than 2%.

IV. RESULTS AND DISCUSSION

A. Differential and total cross sections

We begin our discussion with the results for the neutral channel. In Fig. 3, the predicted differential cross sections of π^0 production are shown in the energy region between 208 and 419 MeV together with experimental results from Refs. [1,2].[2] The displayed cross sections are obtained with a pion photoproduction operator parametrized through the amplitudes A_i and the SAID FA04K solution. One can see one more confirmation of a prediction from Refs. [3,5] that the effect of *np* final-state interaction should lead to a reduction of the cross section and this reduction is the stronger the smaller the pion angles are. This effect is mainly attributed to the strong *np* interaction in the $^3S_1$ wave.

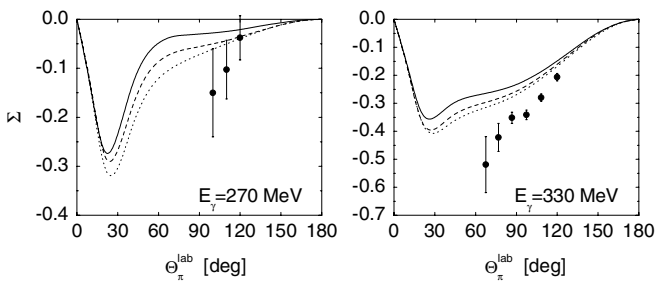

FIG. 15. Angular distribution of the asymmetry Σ for the reaction $d(\gamma, \pi^-)pp$. Notation of the curves as in the middle panel of Fig. 14. Data (preliminary) are from Ref. [40].

Without FSI the model completely fails to reproduce the data. After including FSI, the curves move to the data points although a reasonable description of them still remains to be achieved. At $60^\circ \leqslant \Theta_\pi^{*N} \leqslant 120^\circ$, the predicted cross sections overestimate the data by about 10%–20%.

Possible explanations of the disagreement between the data and the present model can be looked for in the elementary photoproduction operator. As is explained above, the on-shell parametrization for the latter can be used when studying the inclusive channels. Nevertheless, different representations of the operator, which are equivalent in the on-shell case, turn out

[2]In Refs. [1,2] the differential cross sections are given in the so-called "photon-nucleon c.m. frame." Relations needed to transform the cross sections and angles from the γd c.m. frame to the frame mentioned are presented in Refs. [9,10].

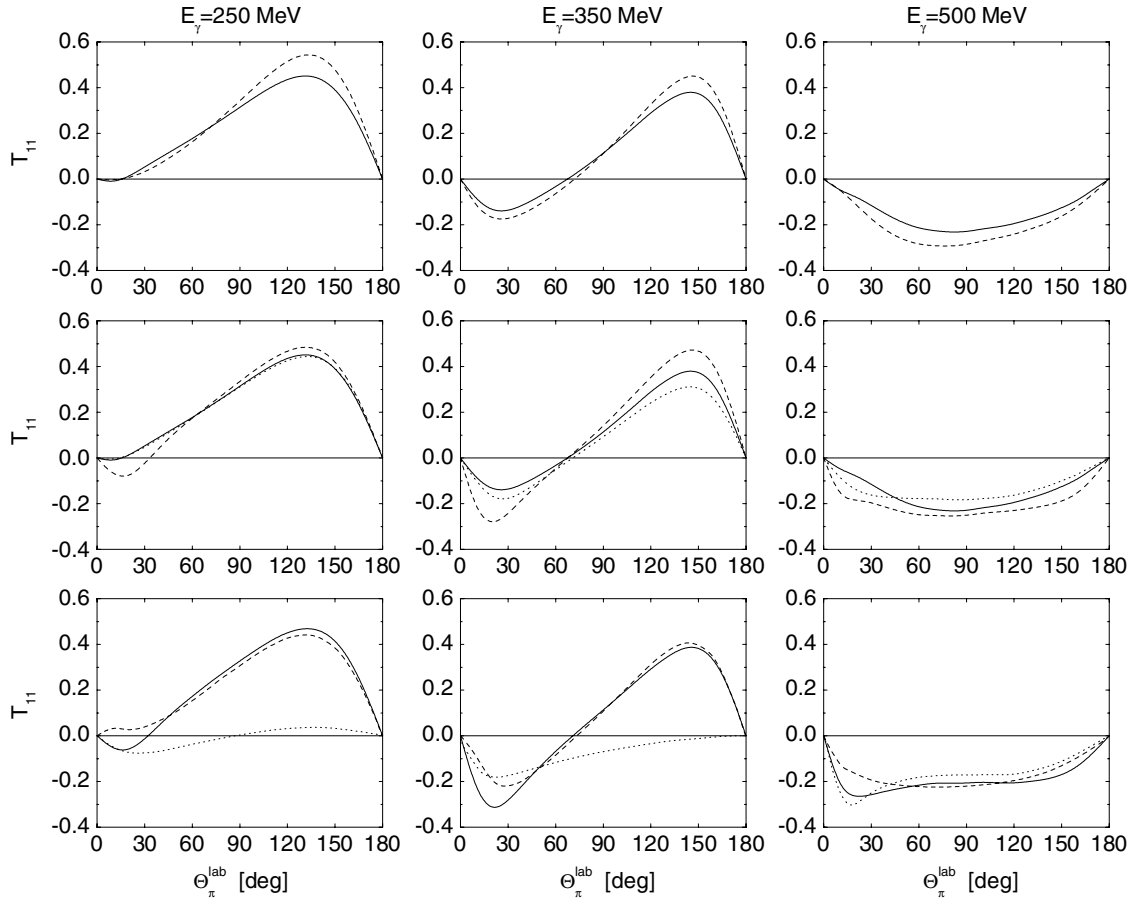

FIG. 16. Target asymmetry T_{11} for the reaction $d(\gamma, \pi^0)np$. Notation of the curves as in Fig. 12.

to be not quite equivalent when one or two nucleons are off their mass shells. Because the sophisticated phenomenological analyses like MAID or SAID provide the elementary amplitude for the on-shell nucleons only, it is hardly possible to give precise quantitative account for the off-shell effects using these amplitudes. One can, however, estimate the possible size of the off-shell effects by performing calculations with different representations of the operator. As an example, we make use of two forms of the operator given in Appendix A, corresponding to the amplitudes A_i (A1) and A'_i (A11). In addition, the MAID03 solution was used to parametrize this operator.

The cross sections, shown in Fig. 4, exhibit quite noticeable dependencies to the different parametrizations of the operator. At 208 MeV, the cross section is sensitive both to the choice of the analysis and the on-shell form of the operator. With increasing photon energy, the sensitivity to the analysis diminishes but the sensitivity to the form of the operator remains to be noticeable. The regions overlapped by the curves can be considered as characterizing the size of possible uncertainties introduced by the pion photoproduction operator. They should be kept in mind at attempts to extract the cross sections on the neutron from deuteron data.

A comparison of our results with those from recent works [11,18] is presented in Fig. 5. Because in the latter article a photoproduction operator was parametrized via the amplitudes A'_i and the MAID03 solution, we give the comparison with the same operator. One can see a satisfactory agreement with the results from Ref. [18]. Slight deviation might be attributed to the use of the different parametrizations for the half-off-shell *NN*-scattering amplitude. At the same time, our differential cross section exhibits quite a different behavior compared to that from Ref. [11]. Reasons responsible for this incongruity of the results can be in the use of both different half-off-shell *NN*-scattering amplitudes and elementary photoproduction operators. We suppose the latter reason to be more probable.

After integrating Eq. (3) over the solid pion angle one obtains the total cross section for a given channel. In Fig. 6, the total cross section for π^0 photoproduction is shown. It is clear that everything told above on the differential cross section also holds true for the total cross section. In particular, one can see that the model without FSI clearly overestimates the data. Inclusion of FSI strongly reduces the cross section although it still noticeable overestimate the data from Refs. [1] and [2] for all parametrizations of an elementary photoproduction operator. Our total cross sections are about 5% higher as compared to those from Ref. [18] in the vicinity of the peak. Note also that in comparison to the prediction from Ref. [11], our peak position is shifted on about 10 MeV to smaller energies that seemingly is because of different elementary photoproduction operators used in two models.

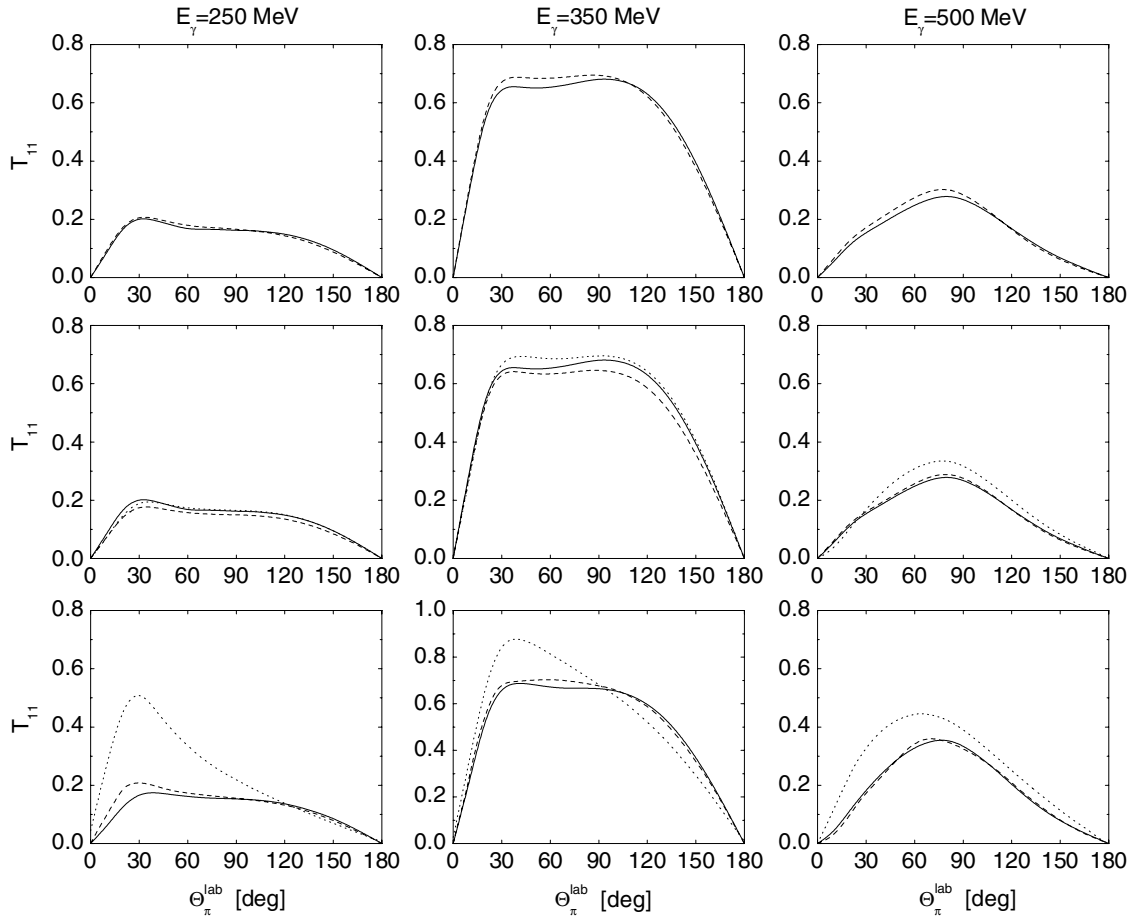

FIG. 17. Target asymmetry T_{11} for the reaction $d(\gamma, \pi^-)pp$. Notation of the curves as in Fig. 14, only in the lower panel, results from Ref. [16] are shown in dotted curves.

In discussion of charged pion photoproduction we restrict ourselves to the $d(\gamma, \pi^-)pp$ channel only because results for the $d(\gamma, \pi^+)nn$ channel are very similar. The dotted curves in Fig. 7 that correspond to the contribution of one pole diagram, reproduce the behavior of the angular dependence for the differential cross section of the elementary reaction $\gamma n \to \pi^- p$. In particular, at energies above 400 MeV, a sharp peak at forward angles because of the pion exchange in the t channel is clearly seen. One can see that at $\Theta_\pi \geqslant 90^\circ$ the cross section from two pole diagrams is practically equal to twice the cross section from one diagram. The reason for this is that at backward angles the events where both nucleons have small momenta correspond to the high momentum components of the deuteron wave function and, therefore, both diagrams cannot work in the quasifree regime at the same time. As a result, the interference term is very small for backward angles. Of course, this conclusion is valid for all channels. In full agreement with a finding from Refs. [11,18], the effect from FSI has only a marginal impact on the differential cross section.

As is seen in Fig. 8, the sensitivity of the cross section to the different parametrizations of the photoproduction operator is not as strong as in the case of the π^0 channel. It remains to be visible only at forward angles.

A comparison of our results with those from recent works [11,18] is presented in Fig. 9. One can see the good agreement with the results from Ref. [18]. We, however, have expected better agreement because the FSI effect is small for the charged channels and, as stated in Sec. III, the results are independent of a choice of DWF. The deviation at forward angles is even somewhat bigger because the Coulomb forces between the protons have been disregarded in Ref. [18]. Their effect consists in the decrease of the cross section on 5%–10% at zero angle in the energy region from 250 to 500 MeV and becomes to be negligible at $\Theta_\pi \gtrsim 30^\circ$. Therefore, reasons for the slight deviations between our results and these from Ref. [18] remain to be investigated. The disagreement with the results from Ref. [11] is also difficult to explain because, as it is stated in Ref. [11], the operator used in that work provides the differential cross sections of the elementary reaction on the nucleon close to those given by the MAID analysis.

The total cross section for π^- photoproduction is shown in Fig. 10. Here the FSI contribution is much smaller than that for π^0 production and leads to a slight decrease of the cross section above 350 MeV. We find satisfactory agreement with data from Refs. [31–33]. At the same time a data point from Ref. [34] at 250 MeV lies markedly below both our predictions and data from Refs. [31,32]. The sensitivity of the results to the choice of the photoproduction operator is rather small. A comparison to the results from Refs. [11,18] shows that three models give very similar results.

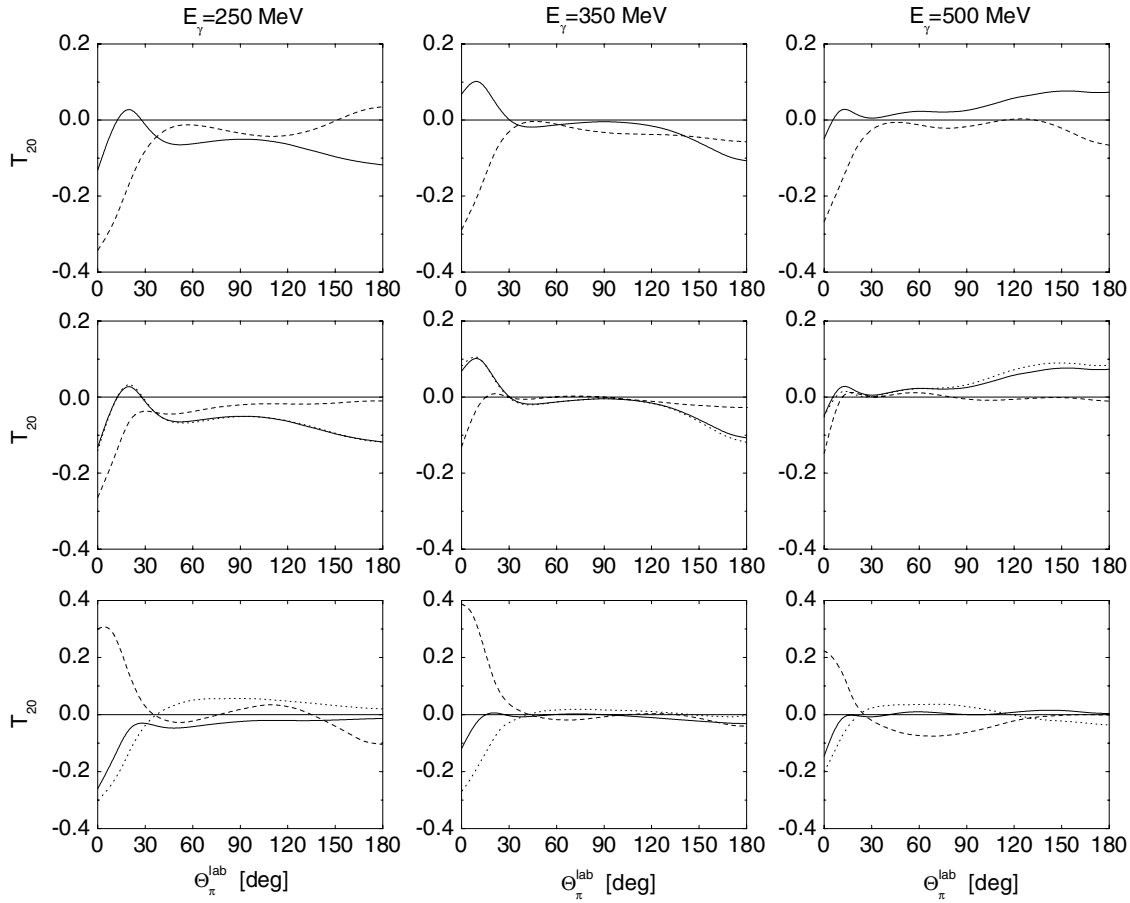

FIG. 18. Target asymmetry T_{20} for the reaction $d(\gamma, \pi^0)np$. Notation of the curves as described in the legend to Fig. 12.

Having results for the total cross sections in all the channels mentioned above one can try to make predictions for the total photoabsorption cross section on the deuteron in the first resonance region. Of course, two more reactions contribute to it as well. These are coherent π^0 photoproduction from the deuteron, $\gamma d \to \pi^0 d$, and deuteron photodisintegration, $\gamma d \to np$. Predictions for the former are taken from a model built in Ref. [35] which provides a good description of data from Ref. [1]. The total cross section for the latter reaction is calculated making use of a phenomenological fit [36] to available experimental data on deuteron photodisintegration up to 440 MeV.

In Fig. 11 we present our results for the total photoabsorption cross section per nucleon for the deuteron. The filled area includes the uncertainties discussed above, because of the variations of the elementary photoproduction operator. It is seen that the predictions even with allowance for these uncertainties are noticeable above the data from Refs. [37,38] in the peak region. In the center of the peak at about 320 MeV we find our prediction of $(543 \pm 7)\,\mu b$ strongly overestimating the experimental value of $(452 \pm 5)\,\mu b$. We have no explanation for this disagreement. There are reasons for the assumption that the total cross sections from Refs. [37,38] may be too low. Such an assumption is supported by the study of other electromagnetic processes. As an example, one can mention that the sum of the electric and magnetic polarizabilities of the neutron calculated with those cross sections turns out to be notably underestimated (see Ref. [39] for a more detailed discussion).

B. Beam asymmetry for linearly polarized photons

The beam asymmetry Σ for π^0 production at three selected energies of 250, 350, and 500 MeV is displayed in Fig. 12. In IA it is negative at all energies. FSI results in a decrease of the magnitude of Σ. The influence from FSI is noticeable at the lowest energy and forward angles. With increasing energy the effect of FSI becomes smaller although not negligible even at the highest energy.

As in case of the differential cross section, the beam asymmetry depends strongly on the form of the elementary production operator. As is seen in Fig. 12, at 250 MeV there exists noticeable sensitivity of Σ to the choice of the analysis of photomeson amplitudes and to the choice of their representations in terms of A_i or A'_i. This sensitivity mainly reflects the difference between the parametrizations FA04K and MAID03 in case of π^0 production near 250 MeV. In the Δ region and at higher energies, the asymmetry is practically independent of the analysis. But here the influence of the choice of the amplitudes A_i or A'_i becomes visible. Only at 350 MeV these amplitudes lead to very close results for the asymmetry. From this finding one may conclude that the

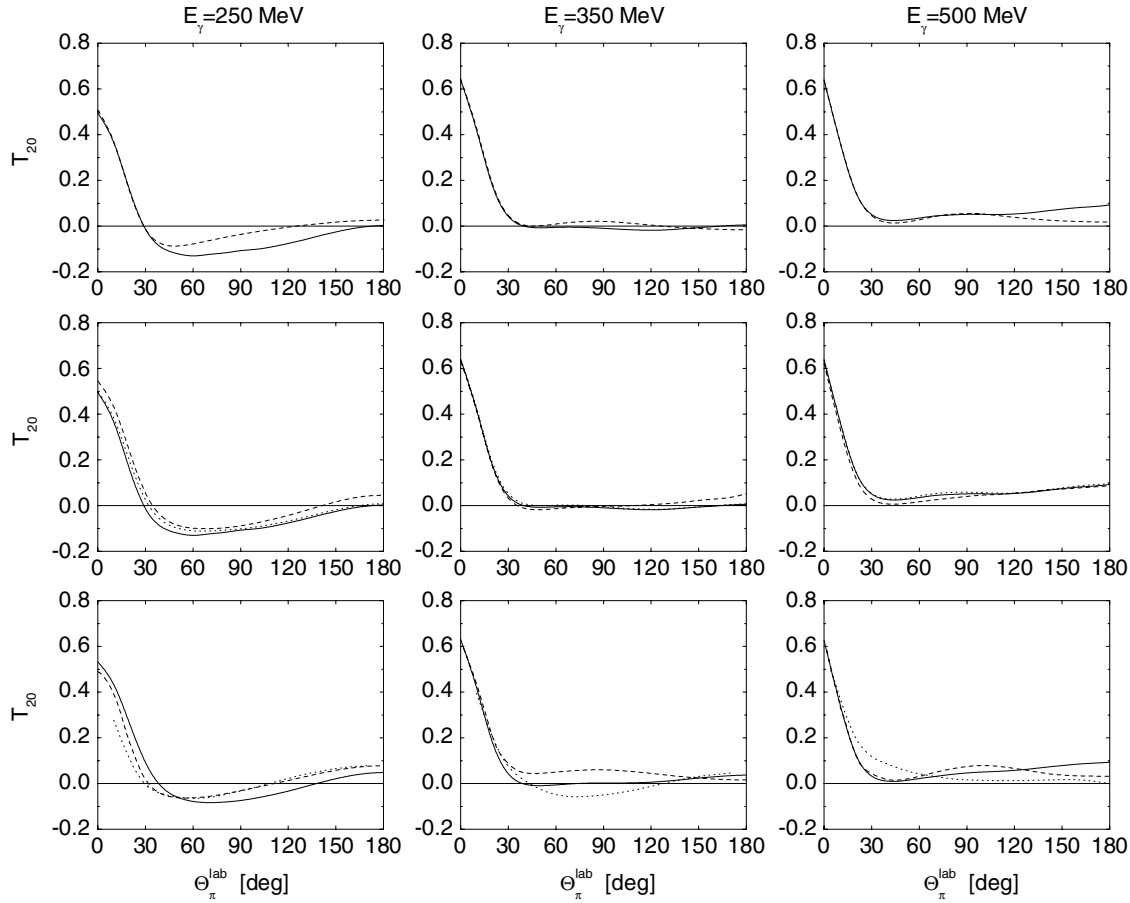

FIG. 19. Target asymmetry T_{20} for the reaction $d(\gamma, \pi^-)pp$. Notation of the curves as described in the legend to Fig. 17.

Δ region is promising for a model independent determination of Σ for the $\pi^0 n$ channel from deuteron data. Outside this region, results of such an extraction will be strongly model dependent.

A comparison of our results with those from Refs. [12,13, 18] is also presented in Fig. 12. Our predictions are similar to those from the latter work although there is a disagreement at forward angles for 250 MeV. As to the predictions from Ref. [12,13], we have a notable disagreement with the results from those works in absolute size of Σ at 250 and 350 MeV and in the form of the angular distribution at 500 MeV. One should mention a strange result of Refs. [12,13] consisting in the statement that Σ does not vanish at $\Theta_\pi = 0$ and π, as it has to be because of helicity conservation [17,18].

Recently first preliminary data on the asymmetry Σ in the π^0 and π^- channels at a few energies between 265 and 330 MeV have been reported by the LEGS collaboration [40]. A comparison with the data for π^0 production is presented in Fig. 13. One can readily see a satisfactory agreement with the experimental values for all parametrizations of the photoproduction operator. Only near 90° the asymmetry is slightly overestimated in absolute size when using the operator built with the SAID model.

The beam asymmetry Σ for π^- production is shown in Fig. 14. Remaining negative as in the case of π^0 production, it shows a quite different behavior. One can see a sharp peak near $\Theta_\pi \approx 30^\circ$. The effect from FSI is much smaller and has a noticeable impact on Σ only at the lowest energy. At the highest energy it is negligible. The SAID and MAID analyses give quite different results for Σ at the lowest energy. This difference diminishes when the energy increases. Notable influence on the predictions at 250 MeV has also the form of the production operator.

In the same figure we compare our predictions to those from Refs. [15,16,18]. Note that polarization observables for the π^- channel were calculated also in Refs. [12,13]. In some cases they are in notable disagreement with those given in Refs. [15, 16]. Authors do not explain reasons for the deviation. In this situation we preferred to make a comparison with predictions from the more recent works. Our results are in reasonable agreement with the predictions of Ref. [18], but in substantial disagreement with the results of Refs. [15,16] both for the form of the angular distribution and for the absolute size of Σ.[3] The disagreement is drastic at the highest energy and can hardly be caused by the use of a different elementary production

[3]In Refs. [15,16] the angular distribution of Σ is given at $E_\gamma = 200$, 270, 330, 370, 420, and 500 MeV. The curves at 250 and 350 MeV displayed in Fig. 14 have been obtained by a quadratic interpolation. The same procedure is used to obtain the target asymmetries $T_{\rm IM}$ for π^- production discussed below.

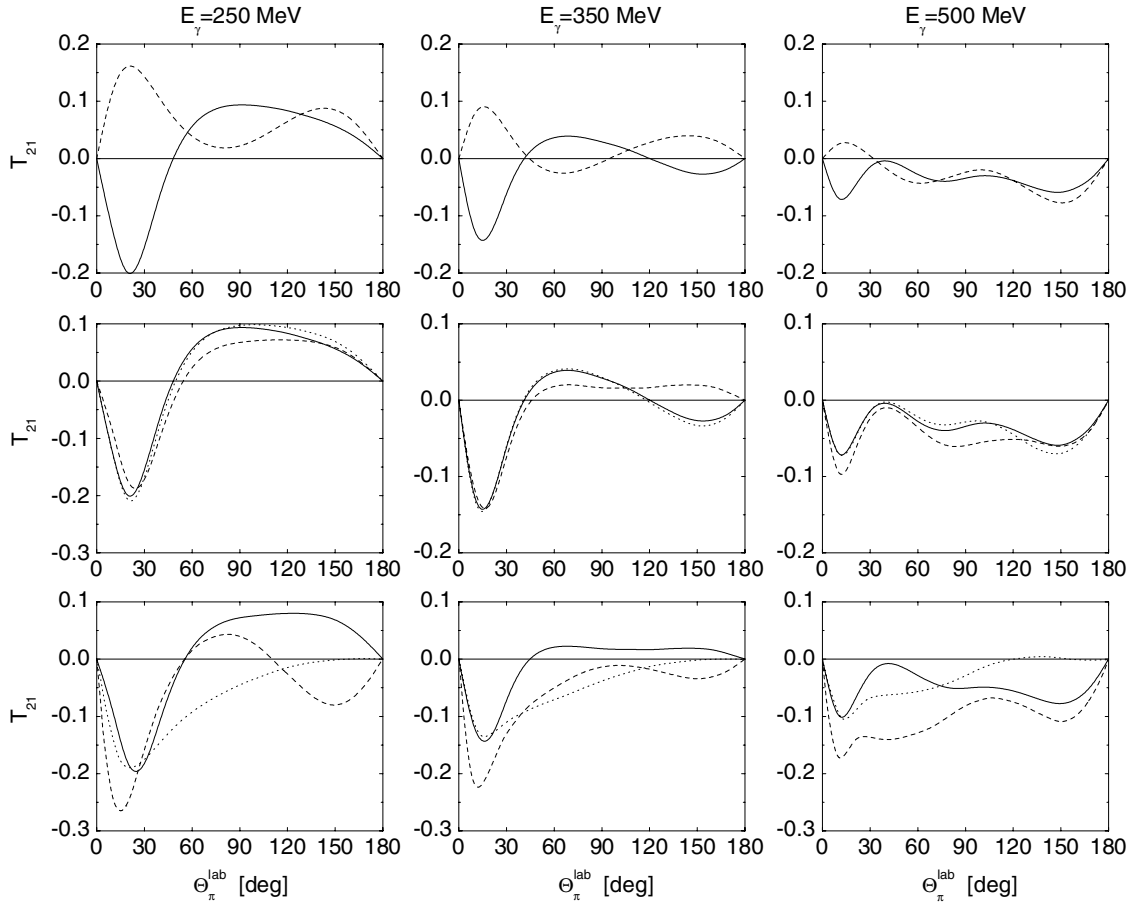

FIG. 20. Target asymmetry T_{21} for the reaction $d(\gamma, \pi^0)np$. Notation of the curves as described in the legend to Fig. 12.

operator. It is likely that there is an unnoticed computational error in Refs. [15,16], leading also to the odd results of nonzero asymmetry at $\Theta_\pi = 0$ and π.

In Fig. 15 we compare our results with the preliminary data from the LEGS collaboration at 270 and 330 MeV. Although some model dependence of the predictions exists, the calculated asymmetry is too small in its absolute size at all the parameterizations of the production operator.

We do not consider here the π^+ channel because all the conclusions just drawn for π^- production remain to be valid for π^+ production as well (see also Ref. [18]) and move to a discussion of the target asymmetries.

C. Target asymmetries for polarized deuterons

The target asymmetries $T_{\rm IM}$ for π^0 and π^- production are shown in Figs. 16–23. The asymmetries for π^+ production are very similar to those in the π^- channel and are not discussed below.

In accordance with results from Ref. [18], we have found that the form of the angular distribution of T_{11} in the π^0 channel changes notable with increasing energy. FSI effects are rather small. The sensitivity of T_{11} to the choice of the photoproduction operator is quite small at the lowest energy. This is not the case at higher energies. The vector asymmetry is sensitive to both the choice of the analysis and the form of the operator. A good agreement of our results with those from Ref. [18] is seen. Only at forward angles $\Theta_\pi \leqslant 30^\circ$ we have found some deviation. The predictions from Refs. [12,13] totally contradict our results both in the form of the angular distribution and in the absolute size at 250 and 350 MeV.[4] For instance, we observe a maximum around 130°–140° at 250 and 350 MeV with $T_{11} \approx 0.4$ in the center of the peak, whereas in Refs. [12,13] the vector asymmetry is close to zero at these energies for $\Theta_\pi \geqslant 90^\circ$. We have no a reasonable explanation for this disagreement. Only at the highest energy one has a good agreement between the three calculations.

Figure 17 shows that FSI effects on the vector asymmetry for π^- production are much smaller than for π^0 production. An analogous result has been reported in Ref. [18]. As in the case of the π^0 channel, the vector asymmetry is practically independent of the photoproduction operator at the lowest energy. At higher energies we observe some sensitivity of T_{11} to that operator especially in the angular region between

[4]When making comparisons to results from Refs. [12,13,16] one should keep in mind that in those works the asymmetry T_{11} is defined with the opposite sign.

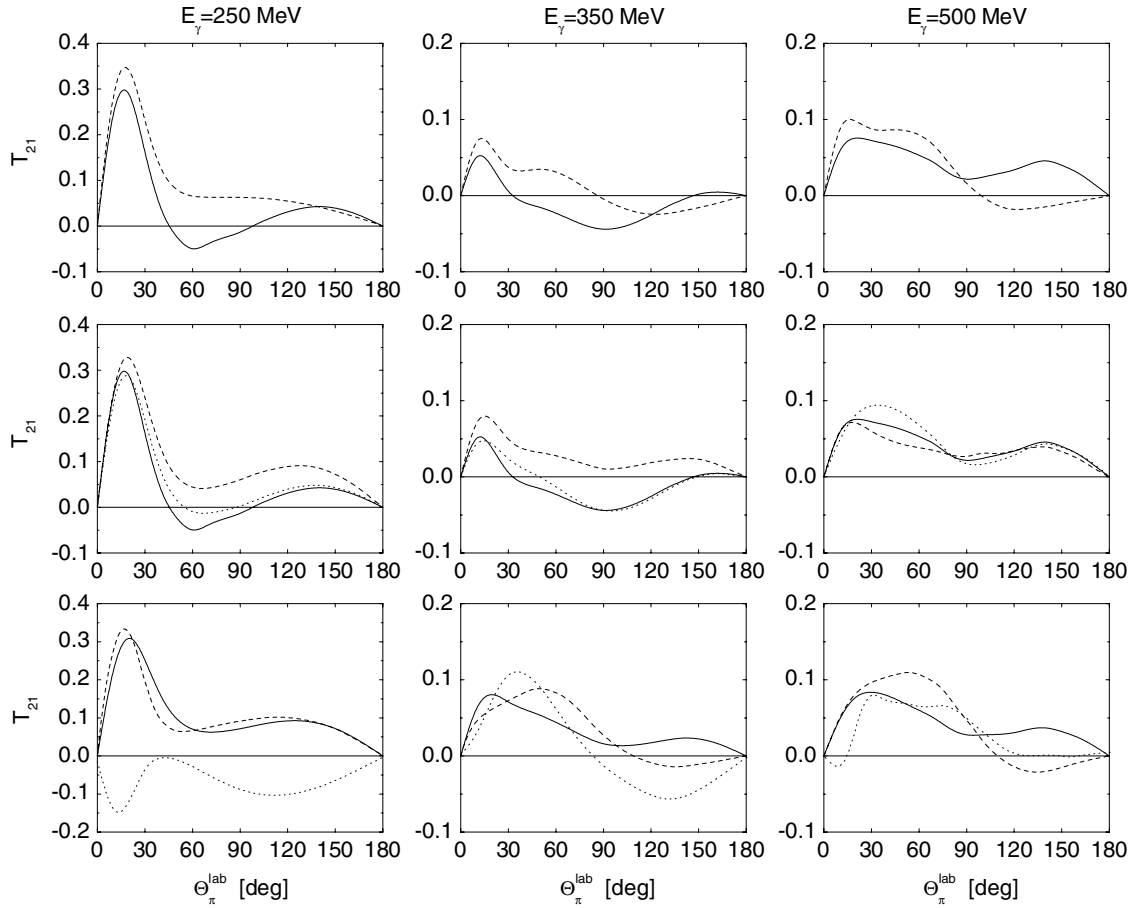

FIG. 21. Target asymmetry T_{21} for the reaction $d(\gamma, \pi^-)pp$. Notation of the curves as described in the legend to Fig. 17.

30° and 120°. One can observe very good agreement with the results of Ref. [18] but significant disagreement with those of Ref. [16] is evident. For instance, we do not find a peak near 30° at 250 MeV predicted in Ref. [16]. In the peak position our value for T_{11} is by a factor of ~ 3 smaller than that in Ref. [16].

The tensor asymmetry T_{20} for π^0 production is displayed in Fig. 18. It is small in absolute size both in IA and IA+FSI. The FSI effect is very large at forward angles as it was previously found also in the case of other observables in the neutral channel. The SAID and MAID models give very close predictions for T_{20} but the results are sensitive to a form of a production operator. The asymmetry T_{20} is the first observable for which we have found a substantial deviation from results of Ref. [18]. Our resulting asymmetry shows a sharp minimum at forward angles, whereas a sharp maximum was found in Ref. [18]. The model [16] predicts even deeper minimum at forward angles than that in our calculation.

As is seen in Fig. 19, the asymmetry T_{20} for the π^- channel is forward peaked in IA. FSI has only a marginal impact on T_{20}. The resulting asymmetry is very small for $\Theta_\pi \geqslant 30^\circ$ especially at high energies. In this kinematic region the results are practically independent of the choice of the production operator. The three approaches predict close peak values of T_{20}. Some deviation takes place in the regions where the asymmetry is small. Note that recently the tensor target asymmetries in π^- photoproduction on the deuteron have been studied in Ref. [41]. Because the authors considered the exclusive reaction, a comparison of our predictions with the results from that work is impossible.

The target asymmetry T_{21} for π^0 production in Fig. 20 shows drastic FSI influence. The resulting absolute size of T_{21} is small. It does not exceed 0.1 for $\Theta_\pi \geqslant 30^\circ$ at all energies and shows a notable model dependence. There exist quite significant differences between the results of our model and those from Refs. [16,18]. As is seen in Fig. 21, practically all the above conclusions remain to be valid for π^- production too. Only at 250 MeV we observe a smaller influence of FSI and a good agreement with the results of Ref. [18] is evident at this energy.

Predictions for the target asymmetry T_{22} for π^0 production are shown in Fig. 22. This asymmetry is very small in IA. Its absolute size is less than 0.03 in the kinematic region under consideration. FSI manifests itself in a pronounced peak around 20° although even in the center of the peak the asymmetry T_{22} is still small being less than 0.12. The sensitivity of T_{22} to the production operator varies with the kinematics. It is quite small at 250 and 350 MeV but becomes to be notable at 500 MeV. It is seen in Fig. 22 that the differences to the results of the three approaches are quite significant.

More pronounced peaks around 20° but in IA are seen in Fig. 23, where the target asymmetry T_{22} for π^- production

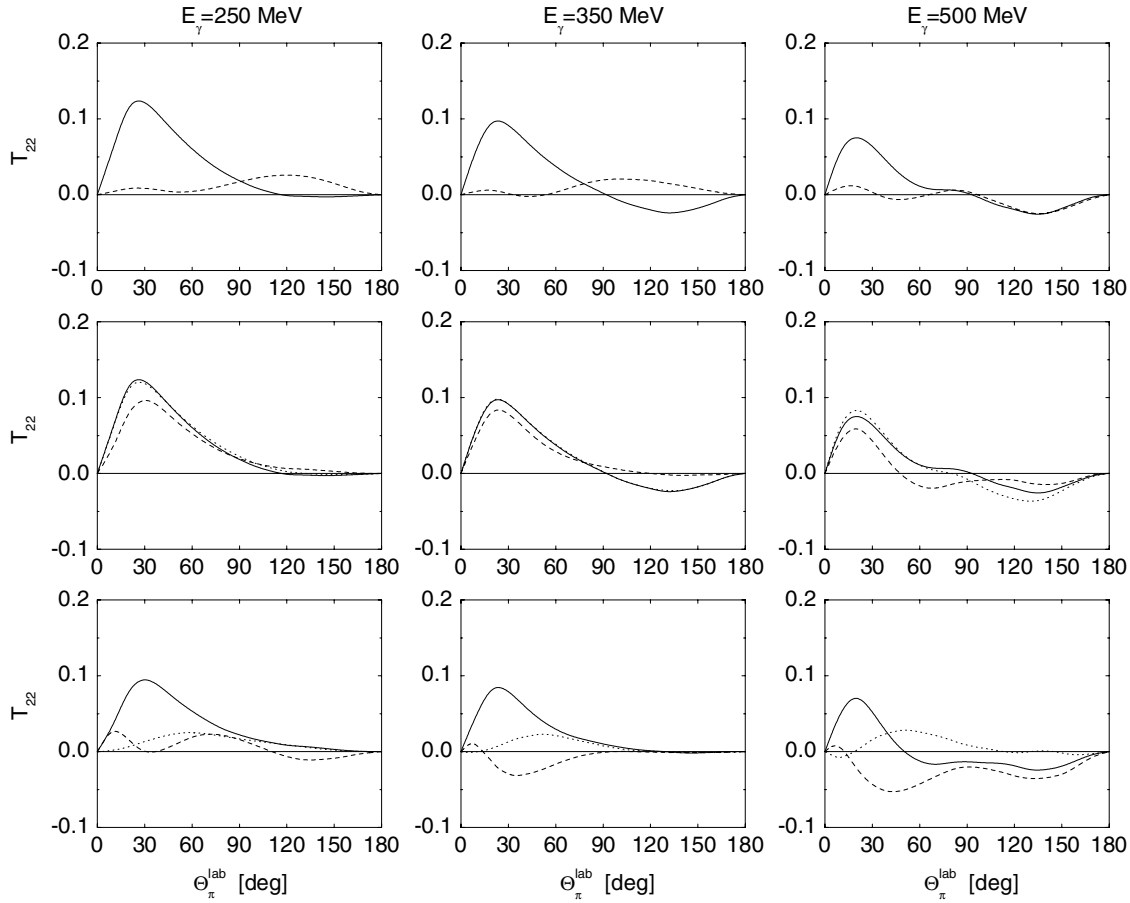

FIG. 22. Target asymmetry T_{22} for the reaction $d(\gamma, \pi^0)np$. Notation of the curves as described in the legend to Fig. 12.

is displayed. The influence of FSI is quite small and seen only at the highest energy for $\Theta_\pi \geqslant 60^\circ$. One notes a sizable dependence of the predictions to the production operator at the lowest energy. It is much smaller at higher energies. We find good agreement with Ref. [18] but significant differences to Ref. [16] are evident at 250 and 350 MeV.

V. SUMMARY AND OUTLOOK

In the present work we have studied incoherent pion photoproduction on the deuteron in the first resonance region taking into account diagrams with a plane-wave final state and with *NN* interaction in the final state. Particular emphasis has been laid on the discussion of possible uncertainties introduced into the model by the elementary operator of pion photoproduction on the nucleon. We have demonstrated that the use of different forms of the on-shell operator has a notable impact on predictions both for the unpolarized cross section and for polarization observables, in particular, the beam and target asymmetries. It is evident that these uncertainties will manifest themselves in the corresponding variations of the amplitude of pion production on the neutron extracted from deuteron data. We have not studied beam-target asymmetries in the present work leaving their consideration for a subsequent publication. However, we are confident that analogous uncertainties will be also seen in these asymmetries.

We have also carried out a detailed comparison of our predictions for unpolarized cross sections and beam and target asymmetries with recent results from Refs. [12,13,15,16,18]. For most observables we have found good agreement with results of the latter work. However, as a rule our predictions are in significant deviation from those in the former works. Of course, part of the disagreement can stem from the use of a different elementary production operator. But in many cases the deviation is too big to have such an explanation so that the reasons for the deviation are still to be understood.

Practically for all parametrizations of the photoproduction operator, our predictions for the unpolarized differential and total cross sections in the π^0 channel are too big in comparison to the available data. The agreement with data in the π^- channel is quite good. The situation with the description of the preliminary data from the LEGS collaboration on the beam asymmetry Σ is opposite. The agreement is satisfactory for π^0 production but our predictions for the π^- channel clearly underestimate the experimental values in absolute size.

An important problem to be solved is the significant disagreement between the theory and experimental data from Refs. [37,38] on the photoabsorption cross section for deuterium in the vicinity of the Δ peak. Even with the allowance for all the uncertainties considered in the present model, we have found our predictions to overestimate significantly the measured values. We suppose that the problem might be in

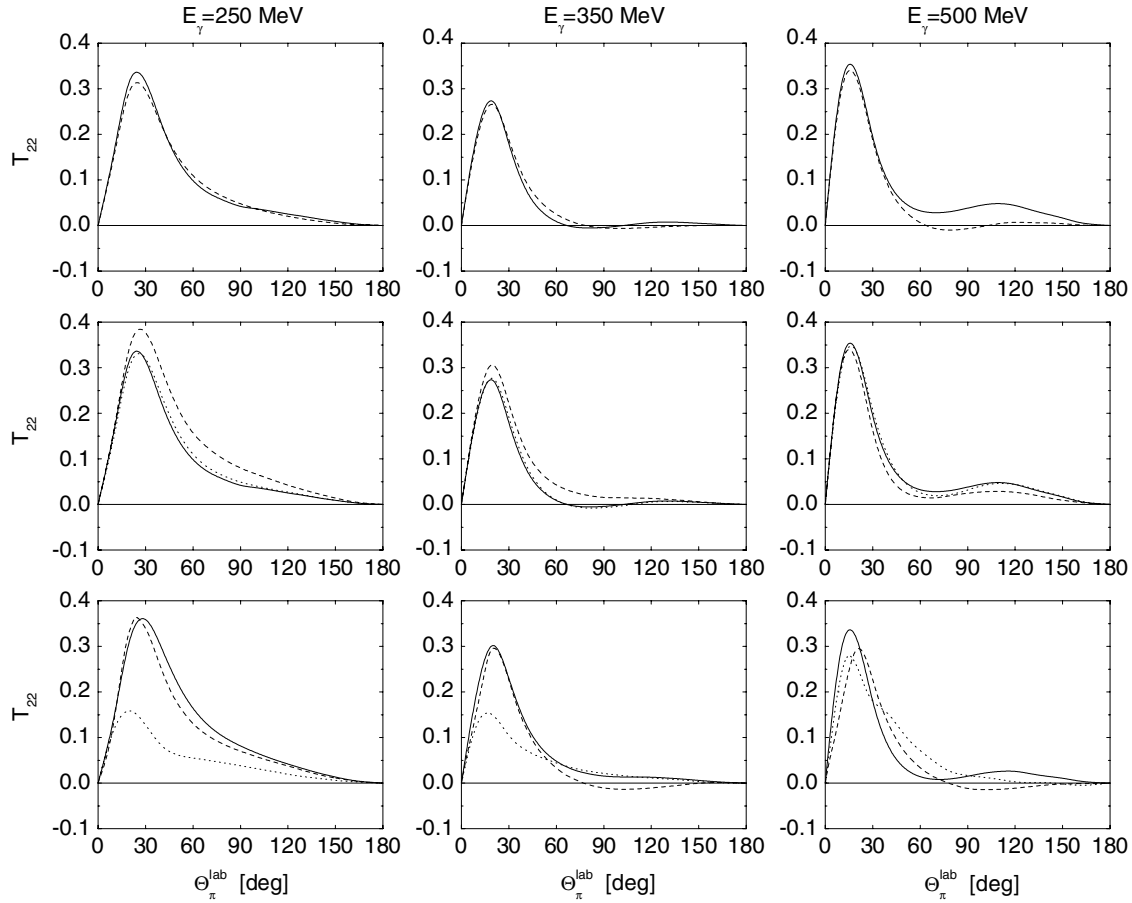

FIG. 23. Target asymmetry T_{22} for the reaction $d(\gamma, \pi^-)pp$. Notation of the curves as described in the legend to Fig. 17.

the data themselves. Using the deuteron values, the authors of Ref. [37] extracted the total photoabsorption cross section on the neutron that, near the Δ resonance energy, is $\sim$20% lower than that presently predicted by the SAID and MAID analyses. New measurements of the deuteron cross section in the peak region would be of very importance to clarify the situation.

Much additional work should be also done to improve the theoretical model. In particular, one should try to take into account two-loop diagrams. As has already been mentioned in Refs. [3,42] for the case of exclusive pion production, there are the kinematic regions where two-loop diagram with *NN* rescattering in the intermediate state can be of importance. However, it is not an easy task to include that diagram in the model for inclusive production because numerical calculations become to be extremely time consuming. Also, in view of the notable sensitivity of the predictions for many observables to the choice of the elementary operator, there is urgent need to develop realistic models which take into account of off-shell effects in pion photoproduction on bound nucleons.

ACKNOWLEDGMENTS

Valuable discussions with A. I. Fix and A. I. L'vov are highly appreciated. We are very grateful to S.S. Kamalov for providing us with the results of his calculations on coherent pion photoproduction on the deuteron and to R. Machleidt for a computer code for the CD-Bonn potential. This work was supported by Belarus RFFR under contracts F05-168 and F05-303, by Deutsche Forschungsgemainschaft under contracts SCHU222 and 436 RUS 113/510, and by the Russian Foundation for Basic Research grant 05-02-17080.

APPENDIX: AN ELEMENTARY PION PHOTOPRODUCTION OPERATOR

The invariant pion photoproduction amplitude can be written as

$$T_{\gamma N\to\pi N'} = \bar{u}(p')\left[\sum_{i=1}^{4} A_i(s,u,t)\Gamma_i\right]u(p), \qquad \text{(A1)}$$

where

$$s=(k+p)^2=(q+p')^2, \quad u=(k-p')^2=(q-p)^2,$$
$$t=(k-q)^2=(p-p')^2, \qquad \text{(A2)}$$

and

$$\begin{aligned}\Gamma_1 &= i\gamma_5 \not\epsilon \not k,\\ \Gamma_2 &= i\gamma_5[q\cdot\epsilon\,(p+p')\cdot k - q\cdot k\,(p+p')\cdot\epsilon],\\ \Gamma_3 &= i\gamma_5(q\cdot k \not\epsilon - q\cdot\epsilon \not k),\\ \Gamma_4 &= \epsilon_{\mu\nu\rho\sigma}\gamma^\mu q^\nu \epsilon^\rho k^\sigma.\end{aligned} \tag{A3}$$

The matrix γ_5 and antisymmetric tensor $\epsilon_{\mu\nu\rho\sigma}$ are fixed according to the conditions

$$\gamma_5 = +\begin{pmatrix} 0 & 1\\ 1 & 0\end{pmatrix} \quad \text{and} \quad \epsilon_{0123} = +1. \tag{A4}$$

In the spinor form, the matrix T reads

$$\langle m_2|T|\lambda m_1\rangle = \langle m_2|L + i\vec\sigma\cdot\vec K|\lambda m_1\rangle. \tag{A5}$$

Contributions of the amplitudes A_i to the matrix T (A5) in an arbitrary frame are as follows

$$\begin{aligned}L_1 &= NN'\left(-\frac{\vec p\cdot\vec S}{E_+} + \frac{\vec p'\cdot\vec S}{E'_+} + \omega\frac{\vec\epsilon\cdot\vec C}{E_+E'_+}\right)A_1,\\
\vec K_1 &= NN'\left[\vec\epsilon\left(\omega + \omega\frac{\vec p\cdot\vec p'}{E_+E'_+} - \frac{\vec p\cdot\vec k}{E_+} - \frac{\vec p'\cdot\vec k}{E'_+}\right)\right.\\
&\quad \left. + \vec k\left(\frac{\vec p\cdot\vec\epsilon}{E_+} + \frac{\vec p'\cdot\vec\epsilon}{E'_+}\right) - \vec p\,\omega\frac{\vec p'\cdot\vec\epsilon}{E_+E'_+} - \vec p'\,\omega\frac{\vec p\cdot\vec\epsilon}{E_+E'_+}\right]A_1,\\
L_2 &= 0,\\
\vec K_2 &= 2NN'(\vec\epsilon\cdot\vec p' p\cdot k - \vec\epsilon\cdot\vec p\, p'\cdot k)\left(\frac{\vec p}{E_+} - \frac{\vec p'}{E'_+}\right)A_2,\\
L_3 &= -NN'\frac{1}{E_+E'_+}(\vec q\cdot\vec\epsilon\vec k\cdot\vec C + q\cdot k\vec\epsilon\cdot\vec C)A_3,\\
\vec K_3 &= NN'\left\{\left(1 - \frac{\vec p\cdot\vec p'}{E_+E'_+}\right)(\epsilon q\cdot k + \vec k\vec q\cdot\vec\epsilon)\right.\\
&\quad + \vec p\left[\left(-\frac{\omega}{E_+} + \frac{\vec p'\cdot\vec k}{E_+E'_+}\right)\vec q\cdot\vec\epsilon + \frac{\vec p'\cdot\vec\epsilon q\cdot k}{E_+E'_+}\right]\\
&\quad \left. + \vec p'\left[\left(-\frac{\omega}{E'_+} + \frac{\vec p\cdot\vec k}{E_+E'_+}\right)\vec q\cdot\vec\epsilon + \frac{\vec p\cdot\vec\epsilon q\cdot k}{E_+E'_+}\right]\right\}A_3,\\
L_4 &= NN'\frac{1}{E_+E'_+}\left[-\vec\epsilon\cdot\vec C\omega\left(E_+ + E'_+\right)\right.\\
&\quad \left. + \vec p\cdot\vec S\left(E'^2_+ + \vec p\cdot\vec p'\right) - \vec p'\cdot\vec S\left(E^2_+ + \vec p\cdot\vec p'\right)\right]A_4,\\
\vec K_4 &= NN'\left\{-\vec\epsilon\left[q^0\left(\frac{\vec p\cdot\vec k}{E_+} - \frac{\vec p'\cdot\vec k}{E'_+}\right) - \omega\left(\frac{\vec p\cdot\vec q}{E_+}\right.\right.\right.\\
&\quad \left.\left.\left. - \frac{\vec p'\cdot\vec q}{E'_+}\right) + \frac{\vec p'\cdot\vec k\vec q\cdot\vec p - \vec p\cdot\vec k\vec q\cdot\vec p'}{E_+E'_+}\right]\right.\\
&\quad + \vec k\left[q^0\left(\frac{\vec p\cdot\vec\epsilon}{E_+} - \frac{\vec p'\cdot\vec\epsilon}{E'_+}\right)\right.\\
&\quad \left. - \frac{\vec\epsilon\cdot\vec p\vec q\cdot\vec p' - \vec\epsilon\cdot\vec p'\vec q\cdot\vec p}{E_+E'_+}\right]\\
&\quad \left. - \vec q\left[\omega\left(\frac{\vec p\cdot\vec\epsilon}{E_+} - \frac{\vec p'\cdot\vec\epsilon}{E'_+}\right) + \frac{\vec C\cdot\vec S}{E_+E'_+}\right]\right\}A_4,\end{aligned} \tag{A6}$$

where $\vec S = \vec k\times\vec\epsilon$, $\vec C = \vec p\times\vec p'$, $E_\pm = E\pm m$, $E'_\pm = E'\pm m$, $N = \sqrt{E_+/2m}$, and $N' = \sqrt{E'_+/2m}$.

The photoproduction operator in the c.m. frame has the well-known form [19]

$$\begin{aligned}\langle m_2|T^*_{\gamma N\to\pi N}|\lambda m_1\rangle &= \frac{4\pi W}{m}\langle m_2|i\vec\sigma\cdot\vec\epsilon^*_\lambda F_1 + \vec\sigma\cdot\hat{\vec q}^*\vec\sigma\\
&\quad\cdot(\hat{\vec k}^*\times\vec\epsilon^*_\lambda)F_2 + i\vec\sigma\cdot\hat{\vec k}^*\hat{\vec q}^*\cdot\vec\epsilon^*_\lambda F_3\\
&\quad + i\vec\sigma\cdot\hat{\vec q}^*\hat{\vec q}^*\cdot\vec\epsilon^*_\lambda F_4|m_1\rangle,\end{aligned} \tag{A7}$$

where $W = \sqrt{s}$ and the superscript asterisk is used for the corresponding quantities in the γN c.m. frame. A comparison of Eq. (A6) in the c.m. frame with Eq. (A7) gives the following relation between the amplitudes F_i and A_i

$$\begin{pmatrix} F_1\\ \frac{E'_+}{q^*}F_2\\ \frac{1}{q^*}F_3\\ \frac{1}{E'_-}F_4\end{pmatrix} = \frac{W_-}{8\pi W}\sqrt{E'_+E_+}\times\begin{pmatrix} 1 & 0 & \frac{q\cdot k}{W_-} & \frac{W^2_- - q\cdot k}{W_-}\\ -1 & 0 & \frac{q\cdot k}{W_+} & \frac{W^2_+ - q\cdot k}{W_+}\\ 0 & W_- & 1 & -1\\ 0 & -W_+ & 1 & -1\end{pmatrix}\begin{pmatrix} A_1\\ A_2\\ A_3\\ A_4\end{pmatrix}, \tag{A8}$$

where $W_\pm = W\pm m$. The inverse relation is as follows

$$\begin{pmatrix} A_1\\ A_2\\ A_3\\ A_4\end{pmatrix} = \frac{4\pi}{q^*\omega^*}\begin{pmatrix} W_+ & -W_- & -2m\frac{q\cdot k}{W_-} & -2m\frac{q\cdot k}{W_+}\\ 0 & 0 & 1 & -1\\ 1 & 1 & \frac{W_-W_+ - q\cdot k}{W_-} & \frac{W_-W_+ - q\cdot k}{W_+}\\ 1 & 1 & -\frac{q\cdot k}{W_-} & -\frac{q\cdot k}{W_+}\end{pmatrix}\times\begin{pmatrix}\sqrt{E_-E'_-}\frac{1}{W_-}F_1\\ \sqrt{E_+E'_+}\frac{1}{W_+}F_2\\ \sqrt{\frac{E_+}{E'_+}}\frac{1}{W_+}F_3\\ \sqrt{\frac{E_-}{E'_-}}\frac{1}{W_-}F_4\end{pmatrix}. \tag{A9}$$

Note that the corresponding formula in Ref. [43] contains misprints for the amplitudes A_1 and A_3. One should emphasize that all variables in Eqs. (A8) and (A9) are taken in the c.m. frame, in particular

$$\begin{aligned}\omega^* &= \frac{s-m^2}{2\sqrt{s}} = \frac{W_+W_-}{2W} = \sqrt{E_+E_-},\\ q^* &= \frac{1}{2W}\sqrt{[W^2-(m+\mu)^2][W^2-(m-\mu)^2]} = \sqrt{E'_+E'_-}.\end{aligned} \tag{A10}$$

Another set of the invariant amplitudes A'_i was used in Ref. [18]

$$T'_{\gamma N\to\pi N'} = \bar u(p')\left[\sum_{i=1}^4 A'_i(s,u,t)\Gamma'_i\right]u(p), \tag{A11}$$

where

$$\Gamma_1' = i\gamma_5 \not\epsilon \not k = \Gamma_1,$$
$$\Gamma_2' = 2i\gamma_5(\epsilon \cdot p' k \cdot p - \epsilon \cdot p k \cdot p') = -\Gamma_2,$$
$$\Gamma_3' = i\gamma_5(\not k \epsilon \cdot p - \not\epsilon k \cdot p),$$
$$\Gamma_4' = i\gamma_5(\not k \epsilon \cdot p' - \not\epsilon k \cdot p'). \tag{A12}$$

There are the following relations between the amplitudes A_i and A_i'

$$A_1' = A_1 - 2mA_4, \quad A_2' = -A_2,$$
$$A_3' = -A_3 - A_4, \quad A_4' = A_3 - A_4. \tag{A13}$$

Using the spinor form of the amplitude T [Eq. (A6)] and that for T' given in Ref. [44], one can show that the difference between T and T' reads

$$T - T' = -A_4 \frac{NN'}{E_+ E_+'} \langle m_2 | \delta \vec{p}' \cdot \vec{S} - \delta' \vec{p} \cdot \vec{S} + i\vec{\sigma} \cdot \{\vec{\epsilon}[\delta(m\omega + p' \cdot k) + \delta'(m\omega + p \cdot k)] + \vec{k}(\delta \vec{p}' \cdot \vec{\epsilon} + \delta' \vec{p} \cdot \vec{\epsilon})\} | \lambda m_1 \rangle, \tag{A14}$$

where $\delta = p^2 - m^2$ and $\delta' = p'^2 - m^2$. Therefore, two representations of the pion production amplitude, Eqs. (A1) and (A11), are equivalent only in the case of on-shell nucleons when $\delta = \delta' = 0$.

[1] B. Krusche, J. Ahrens, R. Beck, M. Fuchs, S. J. Hall, F. Härter, J. D. Kellie, V. Metag, M. Röbig-Landau, and H. Ströher, Eur. Phys. J. A **6**, 309 (1999).
[2] U. Siodlaczek *et al.*, Eur. Phys. J. A **10**, 365 (2001); U. Siodlaczek, Ph.D. thesis, University of Tübungen, 2000.
[3] J. M. Laget, Phys. Rep. **69**, 1 (1981).
[4] R. Schmidt, H. Arenhövel, and P. Wilhelm, Z. Phys. A **355**, 421 (1996).
[5] M. I. Levchuk, V. A. Petrun'kin, and M. Schumacher, Z. Phys. A **355**, 317 (1996).
[6] M. I. Levchuk, M. Schumacher, and F. Wissmann, Nucl. Phys. **A675**, 621 (2000).
[7] I. Blomqvist and J. M. Laget, Nucl. Phys. **A280**, 405 (1977).
[8] J. L. Sabutis, Phys. Rev. C **27**, 778 (1983).
[9] M. I. Levchuk, M. Schumacher, and F. Wissmann, nucl-th/0011041 (unpublished).
[10] E. M. Darwish, Ph.D. thesis, University of Mainz, 2003.
[11] E. M. Darwish, H. Arenhövel, and M. Schwamb, Eur. Phys. J. A **16**, 111 (2003).
[12] E. M. Darwish, Nucl. Phys. **A735**, 200 (2004).
[13] E. M. Darwish, J. Phys. G **31**, 105 (2005).
[14] E. M. Darwish, Nucl. Phys. **A748**, 596 (2005).
[15] E. M. Darwish, Phys. Lett. **B615**, 61 (2005).
[16] E. M. Darwish and A. Salam, Nucl. Phys. **A759**, 170 (2005).
[17] H. Arenhövel and A. Fix, Phys. Rev. C **72**, 064004 (2005).
[18] A. Fix and H. Arenhövel, Phys. Rev. C **72**, 064005 (2005); A. Fix (private communication).
[19] G. F. Chew, M. L. Goldberger, F. E. Low, and Y. Nambu, Phys. Rev. **106**, 1345 (1957).
[20] R. A. Arndt, W. J. Briscoe, I. I. Strakovsky, and R. L. Workman, Phys. Rev. C **66**, 055213 (2002).
[21] D. Drechsel, O. Hanstein, S. S. Kamalov, and L. Tiator, Nucl. Phys. **A645**, 145 (1999).
[22] J. M. Laget, Nucl. Phys. **A296**, 388 (1978).
[23] R. Machleidt, Phys. Rev. C **63**, 024001 (2001).
[24] R. Machleidt, K. Holinde, and Ch. Elster, Phys. Rep. **149**, 1 (1987).
[25] R. Machleidt, Adv. Nucl. Phys. **19**, 189 (1989).
[26] J. Haidenbauer and W. Plessas, Phys. Rev. C **30**, 1822 (1984).
[27] C. M. Vincent and S. C. Phatak, Phys. Rev. C **10**, 391 (1974).
[28] B. Holzenkamp, K. Holinde, and J. Speth, Nucl. Phys. **A500**, 485 (1989).
[29] J. Haidenbauer and K. Holinde, Phys. Rev. C **40**, 2465 (1989).
[30] V. M. Kolybasov and V. G. Ksenzov, Sov. J. Nucl. Phys. **22**, 372 (1976).
[31] P. Benz *et al.*, Nucl. Phys. **B65**, 158 (1973).
[32] G. Chiefari, E. Drago, M. Napolitano, and C. Sciacca, Lett. Nuovo Cimento **13**, 129 (1975).
[33] M. Asai *et al.*, Phys. Rev. C **42**, 837 (1990).
[34] M. A. Quraan *et al.*, Phys. Rev. C **57**, 2118 (1998).
[35] S. S. Kamalov, L. Tiator, and C. Bennhold, Phys. Rev. C **55**, 98 (1997); S. S. Kamalov (private communication).
[36] P. Rossi, E. De Sanctis, P. Levi Sandri, N. Bianchi, C. Guaraldo, V. Lucherini, V. Muccifora, E. Polli, A. R. Reolon, and G. M. Urciuoli, Phys. Rev. C **40**, 2412 (1989).
[37] T. A. Armstrong *et al.*, Nucl. Phys. **B41**, 445 (1972).
[38] M. MacCormick *et al.*, Phys. Rev. C **53**, 41 (1996).
[39] M. I. Levchuk and A. I. L'vov, Nucl. Phys. **A674**, 449 (2000).
[40] Preliminary data of the LEGS Collaboration were taken from Ref. [18].
[41] A. Yu. Loginov, A. A. Sidorov, and V. N. Stibunov, Phys. At. Nucl. **63**, 391 (2000) [Yad. Fiz. **63**, 459 (2000)].
[42] K. Kossert *et al.*, Eur. Phys. J. A **19**, 391 (2004).
[43] A. Salam and H. Arenhövel, Phys. Rev. C **70**, 044008 (2004).
[44] C. Bennhold and H. Tanabe, Nucl. Phys. **A530**, 625 (1991).